Annu. Rev. Mater. Sci. 1997. 27:381–421

CHEMICAL FORCE MICROSCOPY

Aleksandr Noy, Dmitri V. Vezenov, and Charles M. Lieber
Department of Chemistry and Chemical Biology, and Division of Engineering and Applied Sciences, Harvard University, Cambridge, Massachusetts 02138;
email: cml@cmliris.harvard.edu

KEY WORDS: atomic force microscopy, friction, adhesion, self-assembled monolayers, surface free energy, force titration, double layer, imaging

ABSTRACT

Atomic force microscopy is an imaging tool used widely in fundamental research, although it has, like other scanned probe microscopies, provided only limited information about the chemical nature of systems studied. Modification of force microscope probe tips by covalent linking of organic monolayers that terminate in well-defined functional groups enables direct probing of molecular interactions and imaging with chemical sensitivity. This new chemical force microscopy technique has been used to probe adhesion and frictional forces between distinct chemical groups in organic and aqueous solvents. Contact mechanics provide a framework to model the adhesive forces and to estimate the number of interacting molecular groups. In general, measured adhesive and frictional forces follow trends expected from the strengths of the molecular interactions, although solvation also plays an important role. Knowledge of these forces provides a basis for rationally interpretable mapping of a variety of chemical functionalities and processes such as protonation and ionization.

INTRODUCTION

Intermolecular forces affect a variety of problems in condensed phases extending from capillarity and lubrication (1, 2) at macroscopic length scales, micelle and membrane self-assembly on the mesoscopic scale (3), to molecular recognition and protein folding at the nanoscale (4). Understanding these phenomena, regardless of the length scale, requires detailed knowledge of the magnitude and range of intermolecular forces. Atomic force microscopy (AFM) (5) is a powerful tool for probing intermolecular interactions because it can resolve forces

0084-6600/97/0801-0381$08.00

with piconewton sensitivity and has a spatial resolution of nanometers (6). These features enable AFM to produce nanometer to micron scale images of, for example, topography, adhesion, friction, and compliance, and thus make AFM an essential characterization technique for fields ranging from materials science to biology.

The ability to probe interfacial forces with nanometer-scale resolution is critical to developing a molecular-level understanding of a variety of phenomena, including friction and boundary lubrication, adhesion and fracture at interfaces, double-layer forces, and colloid stability. Significantly, the absolute force resolution in AFM can be several orders of magnitude better than the weakest chemical bond (7). This resolution suggests that it should be possible to probe individual molecular interactions, however, the specific chemical groups on a tip interacting with a surface are typically ill-defined. In addition, the contact area of the tip on a surface can be quite large because of finite tip curvature and tip deformation resulting from surface forces (6).

Although force microscopy can provide nanoscale information about friction, adhesion, and compliance, it has not been able to probe directly the specific chemical groups that ultimately determine these phenomena at the molecular level. To overcome this inherent limitation of AFM, we introduced the concept of chemical modification of probes to make them sensitive to specific molecular interactions. By utilizing chemically functionalized tips, force microscopy can be used to (*a*) probe forces between different molecular groups, (*b*) measure surface energetics on a nanometer scale, (*c*) determine pK values of the surface acid and base groups locally, and (*d*) map the spatial distribution of specific functional groups and their ionization state. This ability to discriminate between chemically distinct functional groups has led us to name this variation of AFM chemical force microscopy (CFM) (8).

FORCE MICROSCOPY

Instrumentation and Measurements

A typical force microscope consists of an integrated cantilever-tip assembly interacting with the sample surface, a detector that measures the displacement of the cantilever, and feedback electronics to maintain a constant imaging parameter such as tip-sample separation or force (Figure 1). The integrated cantilever-tip assemblies can have single or V-shaped beams (9) and normal spring constants, k_z, in the range 0.01–100 N/m. The most popular and versatile detection scheme in AFM is optical lever deflection (10). In this scheme, the vertical displacement due to normal forces and the lateral twist due to friction of the cantilever are measured using a quadrant photodiode (11), as shown in Figure 1. Force values are determined from the normal displacement, Δz, or

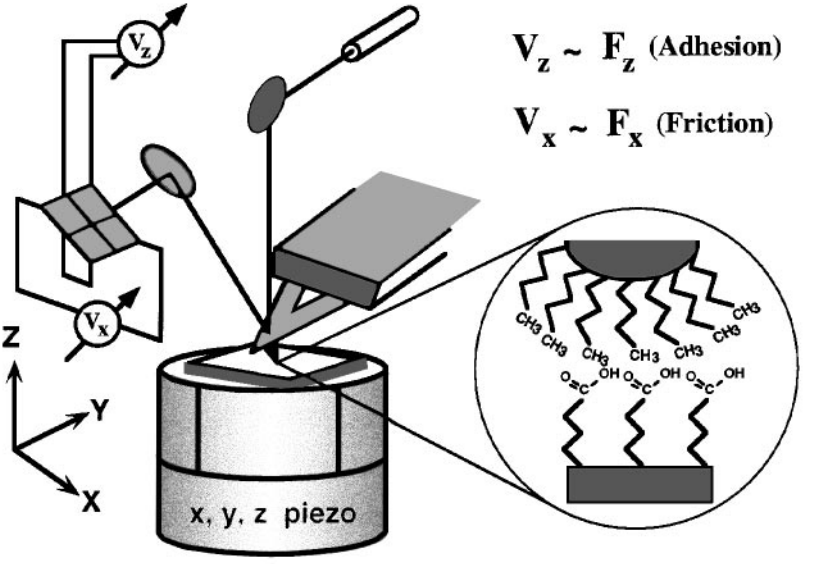

Figure 1 Schematic drawing of the CFM setup. The sample rests on a piezoelectric x, y, z translator. A laser beam is reflected from the backside of the tip onto a photodiode to measure two types of tip-surface interactions. When the sample approaches, touches, and is withdrawn from the tip, the tip will move up and down in response to surface normal forces F_z, resulting in the vertical deflection signal V_z. The cantilever will also twist in response to friction forces $\pm F_x$, yielding the lateral deflection signal V_x. The inset illustrates the chemically specific interactions between a Au-coated, CH_3-terminated tip contacting a COOH-terminated region of a sample.

tilt angle, $\Delta\theta$, of the cantilever from its resting position. With an instrumental sensitivity on the order of 0.1 Å, minimal forces in the range of 10^{-13}–10^{-8} N (depending on the cantilever stiffness) can be measured. Hence, AFM can in principle measure molecular interactions ranging from weak van der Waals ($<10^{-12}$ N) to strong covalent (10^{-7} N) bonds (3). In practice, the displacement (and corresponding force) sensitivity is limited by thermally excited cantilever vibrations and by optical and electronic noise (7). If the measurements are conducted in ambient air or liquids, the thermal noise is especially important. For example, cantilever quality factors drop from 10^3–10^5 in a vacuum to 10^0–10^2 in fluids as a result of hydrodynamic damping. The thermal-noise-limited minimal force is then on the order of 1–20 pN at room temperature.

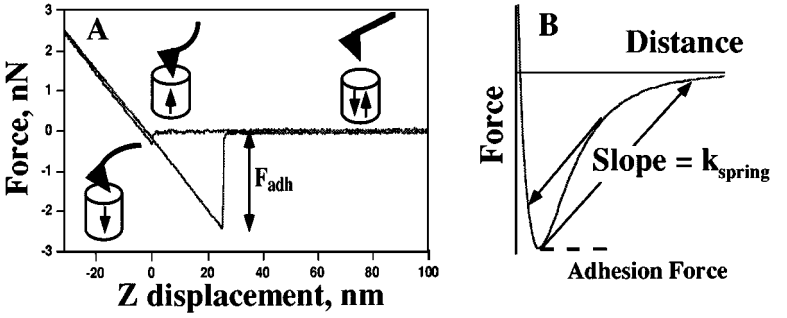

Figure 2 (*A*) Typical force-vs-sample z displacement curve. At large separations, no force is observed between tip and sample. At short distances, the van der Waals attraction will pull the tip abruptly into contact with the sample (jump into contact point). After that, the deflection of the soft cantilever tracks the movement of the sample (linear compliance regime). Hysteresis in the force between tip and sample is observed when the tip is withdrawn from the sample. The finite force necessary to pull the tip off the sample surface corresponds to the adhesive force between functional groups on the surfaces of the tip and sample. (*B*) The cycle in (*A*) is shown in terms of a schematic intermolecular potential between the tip-sample functional groups. Whenever the force gradient exceeds the cantilever spring constant, the system becomes mechanically unstable and cantilever jumps occur.

In principle, the magnitude of intermolecular interactions can be assessed directly in an adhesion measurement (Figure 2). The adhesive interaction between different functional groups is determined from force-versus-sample displacement (F-D) curves. In these measurements, the deflection of the cantilever is recorded during the sample approach-withdrawal cycle (12). The observed cantilever deflection is converted into a force using the cantilever spring constant. The pull-off force determined from the jump in the sample retracting trace corresponds to the adhesion between functional groups on the tip and sample surfaces.

The sphere-on-flat tip-sample geometry of the AFM does not correspond to the interaction between two atoms (Figure 1), although the general features of the interaction potential are the same, that is, the potential has a minimum and increases nonlinearly from this minimum (Figure 2). Because of this nonlinearity, the cantilever experiences mechanical instabilities (i.e. jumps into and out of contact with the sample surface) whenever the tip-surface force gradient exceeds the cantilever spring constant (Figure 2). The magnitude of the adhesion force, which corresponds to the jump out from the force minimum, is measured precisely in these experiments. Ideally, one would like to map the entire potential, which is possible if the effective spring constant can be varied continuously, for example, by applying a variable external force to the tip (13, 14).

Related Techniques

Direct experimental measurement of the interactions between molecules and molecular assemblies has been achieved using other techniques, including the surface forces apparatus (SFA) (15–18), an elastomer lens-on-plate apparatus (19, 20), colloidal probe microscope (21, 22), interfacial force microscope (23), and optical tweezers (24–28). The SFA has yielded considerable information about adhesion and friction between molecular assemblies, although these data are averaged over the large numbers of molecules contained within the approximately 1-mm^2 probing area. Hence, it is difficult to obtain truly microscopic information with this approach. In colloidal probe microscopy, the AFM cantilever is modified with a well-defined micron-size sphere (21). Since the probe radius is better defined than that of sharper microfabricated tips, this approach has an advantage in noncontact experiments. This characteristic of the colloidal probes has been utilized in studies of double-layer interactions (21, 22, 29). However, the large size of the probes used in SFA and colloidal probe microscopy precludes high-resolution mapping of the distributions of these surface forces and the measurement of binding interactions between single pairs of biological molecules.

MEASURING INTERACTIONS BETWEEN MOLECULAR ASSEMBLIES

Tip Modification with Functional Groups

To probe rationally interactions between functional groups the tip must be modified with well-defined molecular layers. This modification can be accomplished by using monolayers of amphiphilic molecules adsorbed on the surface of the tip. Different types of interactions can in principle be studied by varying the head group of the amphiphile. For example, nonspecific adsorption has been used to study long-range forces between hydrophobic (30, 31) and charged (32) surfaces. This approach is limited, however, because physisorbed layers are not very robust. Alternatively, stable molecular layers can be produced by covalently linking the molecular components to the tip and sample surfaces.

We have reported a successful method for covalently modifying AFM tips (8, 33, 34). This method involves self-assembly of monolayers (SAMs) of functionalized organic thiols onto the surfaces of Au-coated Si_3N_4 tips (Figure 3). Stable, robust, and crystalline monolayers of alkyl thiols or disulfides containing a variety of terminal groups can be prepared readily (35–39); thus, it is possible to conduct systematic studies of the interactions between basic chemical groups on the probe tip and similarly modified Au substrates. Covalent modification of AFM probes with thiols and reactive silanes has also been reported

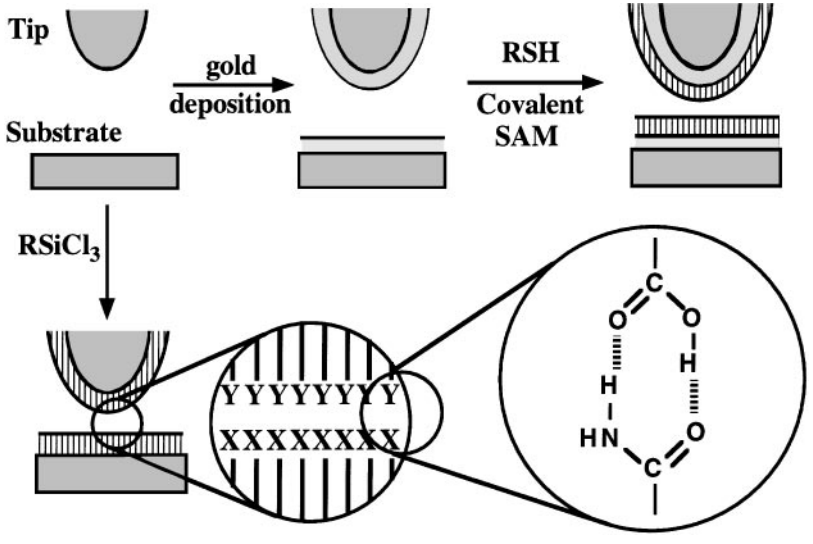

Figure 3 Scheme for chemical modification of tips and sample substrates. Tips and substrates are first coated with a thin layer of Au (50–100 nm) and then, upon immersion in a solution of organic thiol, a dense SAM is formed on the Au surface. Similarly, cleaned Si or Si_3N_4 tips can be derivatized with reactive silanes. The functional groups comprise the outermost surface of the crystalline SAM, and the tip-sample interaction can be fine-tuned by varying the chemistry at the free SAM surfaces. The R in RSH and $RSiCl_3$ represents an organic alkyl chain that ends with a functional group X (X = CH_3, COOH, CH_2OH, NH_2, etc).

by other groups, including studies of adhesion (40–46), contact potential (47), and surface topography (48).

Experimental Environment

The environment in which surfaces interact can play a crucial role in determining measured forces (Figure 4). To probe interactions determined solely by solid-surface free energies (i.e. bare interactions), adhesion forces must be measured in ultrahigh vacuum. Force measurements carried out in ambient air are more difficult to interpret since capillary forces (3, 49) are usually 1–2 orders of magnitude higher than specific chemical interactions. Capillary forces will thus obscure relatively small differences in molecular forces between tip and sample functional groups. On the other hand, capillary condensation will emphasize the relative degree of wetability (hydrophilicity) and can be a basis for discriminating between hydrophobic and hydrophilic groups when imaging under ambient conditions (50). Measurements performed in dry inert gas atmosphere may approach the chemical sensitivity of bare molecular interactions (42, 43); however, caution should be used in interpreting results obtained this

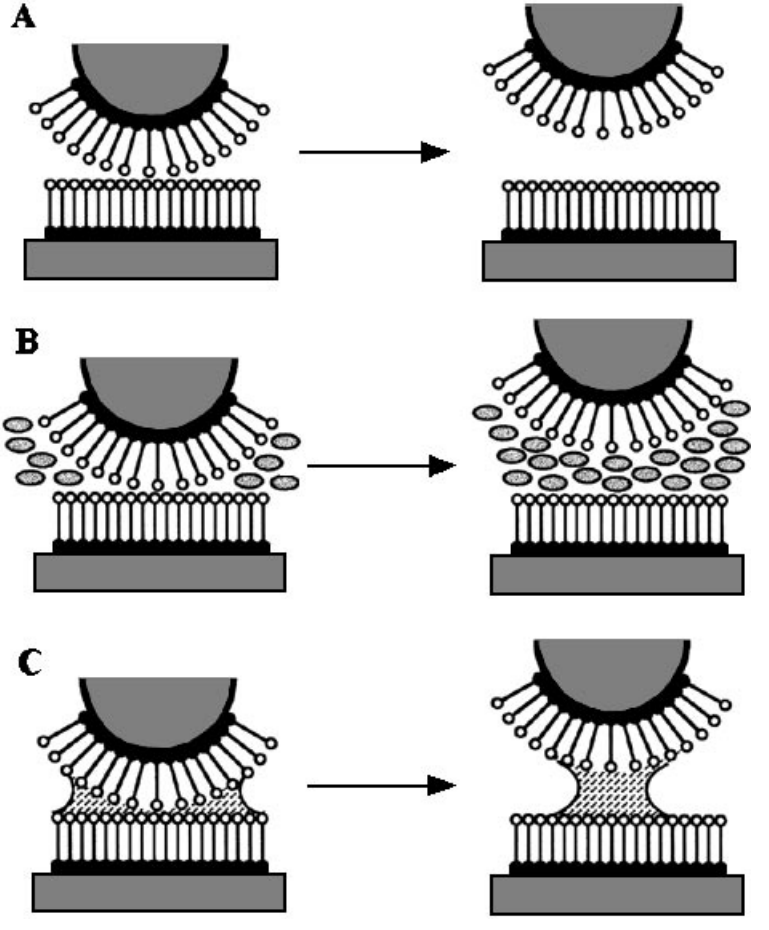

Figure 4 Comparison between force measurements in ultrahigh vacuum, liquids, and ambient air. Interactions under high vacuum conditions are determined by solid surface free energies (*A*). Pulling apart the surfaces under liquid will result in their solvation upon separation. The magnitude of the adhesion force is defined by solid-liquid surface free energies (*B*). Experiments conducted under ambient conditions reflect wetability of the surfaces, since predominant interaction is the result of capillary forces (*C*).

way, because it is difficult to exclude or account for the presence of adsorbed vapor on high-energy surfaces.

The capillary effect can be eliminated by conducting experiments in liquid instead of air (51, 52). Adhesion force measurements with both surfaces immersed in liquid will reflect the interplay between surface free energies of solvated functional groups. Aqueous solution studies are especially important

because AFM is increasingly being used to probe biological systems (53, 54). Indeed, previous AFM studies have found that the images of biomolecules are highly dependent on adhesion forces (55), which can be sensitive to solution pH and ionic strength (56–58) and surface composition (59). It also should be possible to obtain a detailed understanding of these interactions from force microscopy studies if the tip-surface functionality is controlled. This idea is supported by SFA and colloid probe microscopy studies of relatively well-defined but large surfaces (29, 60–62) and by recent CFM studies (34, 63–65).

Probe Characterization and Calibration

To obtain absolute force values and make direct comparisons among studies requires knowledge of the cantilever spring constants and tip radii. Several methods have been reported for experimental calibration of normal spring constants (66–69), k_z. The spring constant can also be calculated for a given cantilever geometry and material (70–72). The Au-coated cantilevers used to prepare SAMs exhibit larger spring constants than do uncoated cantilevers (33) and must be calibrated to reduce uncertainties in the measured forces. The lateral spring constants, k_θ, of cantilevers also can be determined experimentally (73) or derived using the corresponding normal spring constants through the cantilever geometry (33, 70, 71, 74). In addition, the sensitivity of the optical detector, which measures the cantilever displacement, must be calibrated to obtain absolute forces. The normal (z) sensitivity of the detector can be determined from the linear compliance region of the force curve when the tip is pushed against a stiff sample (Figure 2*A*). Noncontact methods have also been described (75, 76). The lateral sensitivity of the detector can be calibrated from atomic stick-slip friction loops (77, 78) or by a noncontact method (79). Alternatively, the lateral sensitivity of a detector also may be related to its normal sensitivity (75, 80, 81).

Finally, the tip radius is an important parameter to characterize, since it affects the contact area between the tip and sample, that is, the number of molecular contacts. Estimates of tip radii are obtained by inspection of electron microscope images (33, 43) or by profiling sharp features (82–86), uniform latex spheres (87, 88), or colloidal gold clusters (89, 90) on the surface.

ADHESION BETWEEN DISTINCT FUNCTIONAL GROUPS

A number of CFM studies of the interactions between different chemical functional groups covalently linked to tips and samples have appeared (Tables 1 and 2) since our initial report of CFM (8). Adhesive forces between tips and substrates modified with SAMs terminating in CF_3, CH_3, OCH_3, CH_2Br, OH, COOH, $COCH_3$, $CONH_2$, and NH_2 groups have been measured in organic (8, 33, 44, 91) and aqueous solvents (34), and in inert dry atmosphere (42, 43).

Table 1 Adhesion forces between functional groups in gaseous environments

No.	Functional group pair (tip-surface)	Monolayer, chain length	Medium	Adhesion (nN)	Ref	Tip radius (nm)
1	COOH-COOH	thiol SAM, C_{16}	dry Ar	62	42	NR(20–40)[a]
2	CH_3-COOH; COOH-CH_3	thiol SAM, C_{16}	dry Ar	≈0	42	NR(20–40)[a]
3	CH_3-CH_3	thiol SAM, C_{18}	dry Ar	≈0	42	NR(20–40)[a]
4	NH_2-COOH	thiol SAM, C_{11}	dry N_2	4.3 ± 0.4[b]	43	100–200
5	COOH-COOH	thiol SAM, C_{11}	dry N_2	1.4 ± 0.3[b]	43	100–200
6	NH_2-NH_2	thiol SAM, C_{11}	dry N_2	0.7 ± 0.2[b]	43	100–200
7	CH_3-CH_3	thiol SAM, C_{11}	dry N_2	0.4 ± 0.2[b]	43	100–200

[a]NR, not reported; a nominal value for similar tips provided by the manufacturer is given in parentheses. Tips were coated with 40 nm of Au.

[b]Adhesion force normalized by the tip radius, F/R, in N/m.

The measured adhesive forces agree with predictions of the Johnson, Kendall, and Roberts (JKR) theory (92), showing that the observed interactions can be linked directly to the surface free energy. Double-layer effects on adhesive forces have also been interpreted in terms of a modified JKR model that incorporates electrostatic interactions (34).

Measurements in Gases

Several studies of functional group interactions have been conducted in dry gases (42, 43) and are summarized in Table 1. The adhesive forces between tips and samples modified with SAMs that both terminate in hydrophobic groups are small (43) or undetectable within the resolution of reported experiments (42). Observed adhesive forces are also small when one of the SAM surfaces terminates with hydrophobic groups and the other terminates with polar groups. In contrast, significant adhesion is observed when both the tip and sample SAM surfaces terminate with hydrogen-bonding groups (Table 1, entries 1, 4–7). The relative magnitudes of the adhesive forces reflect the expected bond strengths, that is, $COOH/NH_2 > COOH/COOH > NH_2/NH_2$. Because the dry gases used in these studies do not preclude adsorption of water and other species on the SAMs, we believe that ultrahigh-vacuum studies will be needed to determine unambiguously the magnitudes of the bare molecular interactions.

Measurements in Organic Solvents

Our CFM experiments carried out in organic solvents probed van der Waals and hydrogen-bonding interactions, whereas those performed in electrolyte solution assessed hydrophobic and electrostatic forces (Table 2). Representative F-D curves obtained in ethanol using Au-coated tips and samples that were

Table 2 Adhesion forces between functional groups in liquid

No.	Functional group pair (tip-surface)	Monolayer, chain length	Medium	Adhesion (nN)	Ref	Tip radius (nm)
1	CH_3-CH_3	silane, C_2	EtOH	0.4 ± 0.3	40	50
2	CH_3-CH_3	silane, C_9	EtOH	0.7 ± 0.6	40	50
3	CH_3-CH_3	silane, C_{14}	EtOH	2.4 ± 1.2	40	50
4	CH_3-CH_3	silane, C_{18}	EtOH	3.5 ± 2.3	40	50
5	CH_3-CH_3	thiol, C_{18}	EtOH	1.0 ± 0.4	33	60
6	CH_3-CH_3	thiol, C_{12}	EtOH	2.3 ± 1.1	44	30
7	CF_3-CF_3	silane, C_{10}	EtOH	15.4	41	NR(20–40)
8	CH_3-CF_3; CF_3-CH_3	silane, C_{18}, C_{10}	EtOH	repulsive	41	NR(20–40)
9	CH_3-CH_3	silane, C_{18}	$CF_3(CF_2)_6CF_3$	52	41	NR(20–40)
10	CF_3-CF_3	silane, C_{10}	$CH_3(CH_2)_6CH_3$	21	41	NR(20–40)
11	CH_3-CH_3	thiol, C_{12}	$CH_3(CH_2)_{14}CH_3$	0.07 ± 0.05	44	30
12	COOH-COOH	thiol, C_{11}	$CH_3(CH_2)_{14}CH_3$	0.11 ± 0.02	44	30
13	COOH-COOH	thiol, C_{11}	$CH_3(CH_2)_4CH_3$	0.95 ± 0.26	91	NR(20–40)[a]
14	COOH-CH_3	thiol, C_{11}, C_{18}	EtOH	0.3 ± 0.2	33	60
15	COOH-COOH	thiol, C_{11}	EtOH	2.3 ± 0.8	33	60
16	COOH-COOH	thiol, C_{11}	EtOH	0.27 ± 0.04	44	30
17	COOH-COOH	thiol, C_{11}	PrOH	1.37 ± 0.26	91	NR(20–40)[a]
18	CH_2OH-CH_2OH	thiol, C_{11}	EtOH	0.18 ± 0.18	44	30
19	COOH-COOH	thiol, C_{11}	H_2O	2.80 ± 0.20	91	NR(20–40)[a]
20	COOH-COOH	thiol, C_{11}	H_2O, pH < 5[b]	7.0 ± 0.2	34	60
21	COOH-COOH	thiol, C_{11}	H_2O, DI	2.3 ± 1.1	44	30
22	COOH-CH_2OH	thiol, C_{11}, C_{11}	H_2O, pH < 5[b]	1.1 ± 0.5	34	30
23	CH_2OH-CH_2OH	thiol, C_{11}	H_2O[b]	1.0 ± 0.2	34	20
24	CH_2OH-CH_2OH	thiol, C_{11}	H_2O, DI	0.30 ± 0.05	44	30
25	CH_3-CH_3	thiol, C_{18}	H_2O	60 ± 5	34	60
26	CH_3-CH_3	thiol, C_{12}	H_2O	12.5 ± 4.4	44	30

[a]Tips were coated with 50 nm of Au.

[b]Ionic strength IS = 0.01 M.

functionalized with SAMs terminating in CH_3 or COOH groups reveal the difference between the individual interactions (Figure 5).

To quantify the differences and uncertainties in the adhesive interactions between different functional groups, however, it is necessary to record multiple force curves for each type of intermolecular interaction. Histograms of the adhesive force versus the number of times this force is observed typically exhibit Gaussian distributions (Figure 6) and yield mean adhesion forces (± experimental uncertainty) of 2.3 ± 0.8, 1.0 ± 0.4, and 0.3 ± 0.2 nN for interactions between COOH/COOH, CH_3/CH_3, and CH_3/COOH groups, respectively. Since the mean values do not overlap, these chemically distinct functional groups may be differentiated by measuring the adhesion forces with a tip that terminates in a defined functionality. The observed trend in the magnitudes of the adhesive

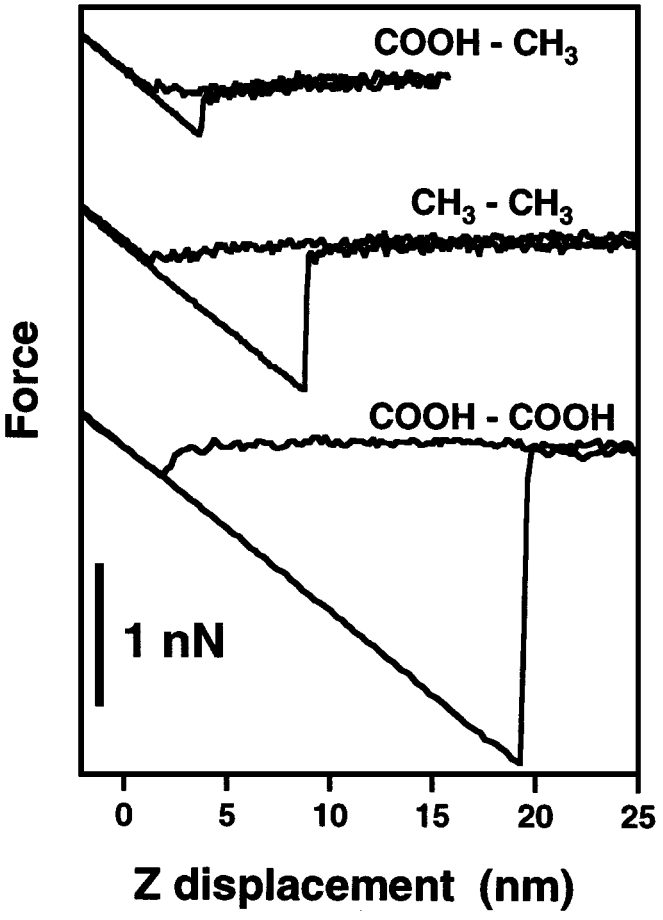

Figure 5 Representative F-D curves in ethanol recorded for COOH/COOH, CH_3/CH_3, and CH_3/COOH tip-sample functionalization (tip R $\sim$ 60 nm) (reproduced from Reference 33).

interactions between tip/sample functional groups, that is COOH/COOH > CH_3/CH_3 > CH_3/COOH, agrees with the qualitative expectation that interactions between hydrogen-bonding groups (i.e. COOH) will be greater than between non-hydrogen-bonding groups (i.e. CH_3). The forces observed in dry, inert gas between these and similar functional group combinations parallel our results in ethanol solvent (42, 43).

When the solvent is chemically similar to the tip and sample terminal functional groups (e.g. CH_3 groups in hexadecane or CH_2OH groups in ethanol),

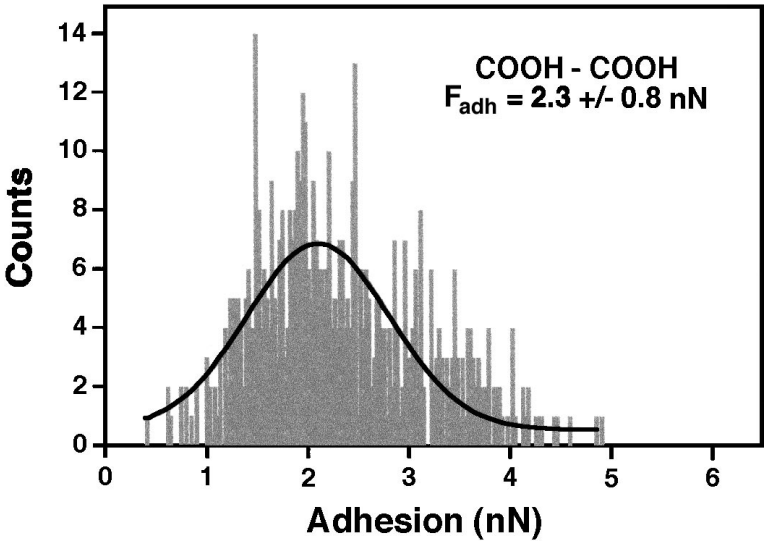

Figure 6 A histogram showing the number of times that a given adhesion force was observed in repetitive measurements using COOH-terminated samples and tips. The histogram represents approximately 400 tip-sample contacts for one functionalized tip in ethanol (adapted from Reference 33).

the forces required to separate the tip and surface are small (Table 2, entries 11 and 18). Cross-interactions between immiscible components were either very small (e.g. CH_3/COOH in ethanol) or even repulsive (e.g. CH_3/CF_3 in ethanol). In contrast, when the solvent is immiscible with the functional groups that terminate the SAMs on the tip and sample, the adhesive forces are extremely large. Both van der Waals (Table 2, entries 9 and 10) and hydrophobic (Table 2, entries 25 and 26) interactions can be responsible for this latter behavior.

Continuum and Microscopic Models

JKR MODEL Adhesion data can be used to assess the energetics of the different intermolecular interactions and to estimate the absolute number of functional groups contributing to experimentally observed forces. This assessment requires consideration of the contact deformations between tip and surface. If no molecular forces are present, the tip will separate from the sample without adhesion (Figure 7, Hertz). In cases of observed adhesion, the JKR theory of adhesion mechanics (3, 92) can be used to assess quantitatively the above two points. This model assumes contact range surface forces (Figure 7) and predicts that the pull-off force, F_{ad}, required to separate a tip of radius R from a planar

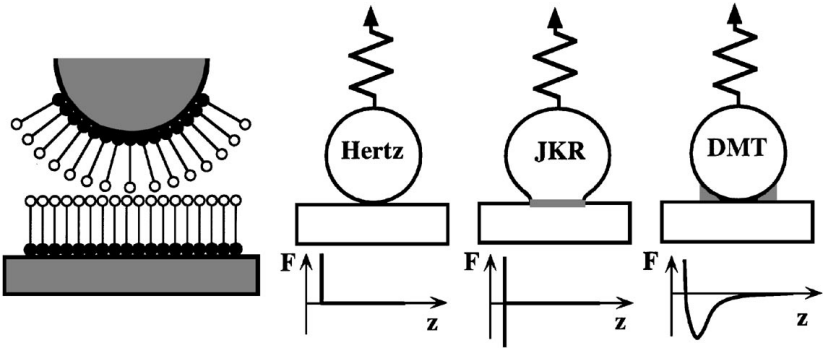

Figure 7 Deformation of a spherical tip on a flat substrate at pull-off and corresponding force profiles according to contact mechanics models.

surface will be given by

$$F_{ad} = \frac{3}{2}\pi R W_{SMT}, \quad 1.$$

where

$$W_{SMT} = \gamma_{SM} + \gamma_{TM} - \gamma_{ST} \quad 2.$$

is the thermodynamic work of adhesion for separating the sample and tip; γ_{SM} and γ_{TM} are the surface free energies of the sample (S) and tip (T), respectively, in contact with the medium M [vacuum, vapor (V) or liquid (L)] and γ_{ST} is the interfacial free energy of the two contacting solid surfaces. Self-consistent calculations (93) indicate that deformations at this scale are unimportant, and thus

$$F_{ad} = 2\pi R W_{SMT}. \quad 3.$$

This formula is the well-known result of the Derjaguin, Muller & Toporov (DMT) theory (94), which assumes finite–range surface forces and no deformation, that is, zero contact area at the moment when bonds between functional groups on the tip and sample rupture (Figure 7). The exact value of the numerical coefficient in Equation 1 (3/2 vs 2) is beyond the experimental uncertainty (width of adhesion force distribution plus errors in determination of k and R; see Tables 1 and 2), and both approaches have been used to derive surface free energies from adhesion data. However, even when the work of adhesion is given more accurately by the DMT expression, the surface profile and contact area are better described by the JKR model (95, 96). Use of the JKR model to correlate adhesion force and surface free energy also allows for estimates of the number of interacting groups.

If the sample and tip bear identical functional groups (e.g. CH_3/CH_3 interactions), then $\gamma_{ST} = 0$ and $\gamma_{SL} = \gamma_{TL}$, and Equation 2 simplifies to $W_{SMT} = 2\gamma$, where γ corresponds to the free energy of the surface in equilibrium with vapor phase or solvent. Therefore, the solid-vapor or solid-liquid surface free energy should determine the adhesive force between tip and sample pairs modified with the same molecular groups.

This approach can be checked by independently calculating the expected value of F_{ad} for CH_3-terminated surfaces and tips. Previous measurements of the contact angle (CA) of ethanol on CH_3-terminated SAMs (37) yielded a value of $\gamma = 2.5$ mJ/m^2. The value of $F_{ad} = 1.2$ nN calculated using this value of γ and the experimentally determined tip radius agrees well with the measured value of 1.0 ± 0.4 nN. Thus this continuum approach provides a reasonable interpretation of microscopic CFM measurements. Additional verification comes from experiments in several different solvents (44). In this case, γ_{SL} and, hence, F_{ad} are directly proportional to $\gamma_{LV}\cos(CA)$. Plots extrapolated to zero adhesion force yield γ_{SV}. We have used this approach and reported data for CH_3-terminated SAMs (44) to obtain a value of γ_{SV}, 22 ± 6 mJ/m^2, in close agreement with the value of 19.3 mJ/m^2 reported by Bain et al (37).

Alternatively, this analysis can yield important information about the surface free energies in cases where conventional contact angle measurements fail to yield γ. In particular, contact angle measurements cannot be used to probe high free energy surfaces that are wet by most liquids. Adhesion measurements are free of this limitation, and moreover, high surface energies lead to larger (easily measured) forces. For COOH-terminated SAMs, CFM data yield a value of $\gamma = 4.5$ mJ/m^2 in ethanol. The interactions between hydrogen-bonding groups in inert gas atmosphere are of considerably larger magnitude than in ethanol (Table 1). It remains unclear, however, whether these latter values of γ_{SV} are representative of true solid-surface free energies, since the amount of vapor adsorbate is ill-defined. Solvation would reduce the observed $\gamma_{SV(obs)}$, whereas capillary contribution would increase $\gamma_{SV(obs)}$ relative to the true value.

Another unique application of CFM is in the determination of interfacial free energies, γ_{12}, between two different solid surfaces. By first determining γ values for homogeneous interactions, γ_{12} can be determined using Equation 2 and relevant F_{ad} values from experiment. Examples include the $COOH/CH_3$ pair in ethanol and the $COOH/NH_2$ pair in dry nitrogen. In the first case, a small adhesion force is consistent with a high value of γ_{12} (5.8 mJ/m^2). In the second case, significant attractive force apparently results from a large negative value of γ_{12} (-518 mJ/m^2). In short, this means that acid-base interactions across an interface are much stronger than is hydrogen bonding between acid or base separately, and that termination of a hydrogen-binding interface (COOH) with a non-hydrogen-binding (CH_3) interface is unfavorable.

ROLE OF THE SOLVENT The role that solvation plays in these adhesion measurements can be probed further by using the Fowkes-van Oss-Chaudhury-Good (FOCG) surface tension component model (97–99). In this model, the total surface tension of a polar system is separated into dispersion γ^{LW} (Lifshitz–van der Waals), Lewis acid γ^+, and base γ^- components:

$$\gamma_{total} = \gamma^{LW} + \gamma^{AB}, \qquad 4.$$

where $\gamma^{AB} = 2\sqrt{\gamma^+\gamma^-}$. The work of adhesion between identical surfaces, S, immersed in liquid, L, then becomes

$$W_{SLS} = 2\gamma_{SL} = 2\Big[\Big(\sqrt{\gamma_L^{LW}} - \sqrt{\gamma_S^{LW}}\Big)^2 + 2\Big(\sqrt{\gamma_L^+\gamma_L^-} + \sqrt{\gamma_S^+\gamma_S^-} - \sqrt{\gamma_L^+\gamma_S^-} - \sqrt{\gamma_S^+\gamma_L^-}\Big)\Big]. \qquad 5.$$

With completely apolar surfaces, such as the CH_3-terminated SAMs, the last three terms in Equation 5 are zero (i.e. $\gamma^{AB} = \gamma^+ = \gamma^- = 0$). The dispersion component of CH_3-terminated SAMs determined from contact angle measurements with liquid hydrocarbons is 19.3 mJ/m^2 (37). This value is essentially the same as the $\gamma^{LW} = 20.1$ mJ/m^2 for ethanol (97). Thus, the first term in Equation 5 is also negligible, and the value of the adhesion force between two methyl surfaces in ethanol is essentially a measure of the strength of the hydrogen-bonding interaction between ethanol molecules:

$$W_{CH_3/EtOH/CH_3} = 2\gamma_{EtOH}^{AB}. \qquad 6.$$

From the total surface tension of ethanol (22.75 mJ/m^2), we conclude that the CH_3 SAM/ethanol interfacial tension, $\gamma_{CH_3/EtOH}$, derived from force measurements should be $\gamma_{CH_3/EtOH} \approx \gamma_{EtOH}^{AB} = 2.65$ mJ/m^2. This value compares favorably with the 2–4 mJ/m^2 value determined from adhesion experiments (Table 2, entries 3–6). Corroboration of this interpretation comes from comparisons of the adhesion forces in ethanol and methanol, since these solvents have virtually identical surface tensions [22.75 and 22.61 mJ/m^2, respectively (100)] but different hydrogen bonding [$\gamma^{AB} = 2.65$ and 4.11 mJ/m^2, respectively (97)]. By exchanging solvents with the same tip and sample we found that forces between CH_3 groups in MeOH are consistently 1.5–2 times greater than those in EtOH, in agreement with the ratio of 1.6 between corresponding γ^{AB} values.

This model also predicts that adhesion measurements made in a nonpolar or monopolar solvent (e.g. such that $\gamma^+ = 0$) with surface tension close to that of the CH_3-terminated SAMs should be very small. Indeed, we observed in ethyl acetate ($\gamma = 23.9$ mJ/m^2) that adhesion forces could not be determined within the noise level of our experiment (<0.01 nN). Other examples

are ethyleneglycol (EG) and dimethylsulfoxide (DMSO). These solvents have significant acid-base components (19 and 4 mJ/m^2, respectively) and dispersion contributions differing from that of the CH_3-terminated SAM (29 and 36 mJ/m^2, respectively) (97). Adhesive forces between methyl surfaces in EG are predicted (Equations 4 and 5) to be greater than those in DMSO by a factor of 3.0, whereas experiments yield a difference factor of 2.8 (DV Vezenov, A Noy, CM Lieber, unpublished results). These data independently confirm the validity of the FOCG approach for treating the interactions in solvents.

Similarly, assuming that the γ^{LW} component is approximately the same for both methyl- and acid-terminated SAMs, the work of adhesion between the other two possible functional group combinations in ethanol is given by:

$$W_{COOH/EtOH/COOH} = 2\gamma^{AB}_{COOH/EtOH} \quad 7.$$

$$W_{CH_3/EtOH/COOH} = \gamma^{AB}_{COOH/EtOH} - \Delta\gamma^{AB}_{COOH/EtOH}, \quad 8.$$

where $\gamma_{COOH/EtOH}$ represents interfacial free energy and $\Delta\gamma^{AB}_{COOH/EtOH} = \gamma^{AB}_{COOH} - \gamma^{AB}_{EtOH}$. This analysis suggests that the small magnitude of the adhesion force between CH_3/COOH-terminated SAMs in ethanol results from the similarity in the hydrogen-bonding energetics for the COOH/EtOH system.

NUMBER OF MOLECULAR CONTACTS The JKR model can also provide an estimate of the number of molecular interactions contributing to the measured adhesive forces. The contact radius at pull-off, a, for surfaces terminating in the same functional groups is

$$a = (3\pi\gamma R^2/K)^{1/3}, \quad 9.$$

where $K = (2/3)[E/(1 - \nu^2)]$ is the effective elastic modulus of the tip and sample, E is the Young modulus, and ν is the Poisson ratio. The value of K can be approximated by the bulk value for Au [64 GPa (101)], since the thin SAMs do not significantly change the elastic behavior of the tip material, that is, $E_{Au/SAM} = (E_{Au}t_{Au} + E_{SAM}t_{SAM})/(t_{Au} + t_{SAM}) \approx E_{Au}$, where t is the layer thickness. Equation 9 yields $a = 1.0$ nm and a contact area of 3.1 nm^2 for the CH_3/CH_3 interaction in ethanol. Since the area occupied by a single functional group of close-packed thiolate SAMs on Au is 0.2 nm^2 (102), this result corresponds to an interaction between only 15 molecules on the tip and sample. A similar analysis of the COOH/COOH data from ethanol shows that the adhesive interaction is determined by 25 molecular contacts. Ultimately, this analysis predicts that when the tip radius is reduced to $R < 10$ nm, the contact area at pull-off will correspond to the interaction between a single molecular pair. Measurements with ultrasharp tips could be used to test this prediction and the validity of using a continuum theory for microscopic measurements;

however, disorder in the SAM on highly curved tips (103) may preclude the use of this approach in measuring interactions between single molecular pairs.

Adhesion in Aqueous Solutions

Water is another important medium for CFM experiments. The acid-base chemistry of ionizable sites immobilized at interfaces spans several systems, such as colloids, micelles, polymers, polyelectrolytes, and biological macromolecules. The dissociation constants of the surface groups in these systems often differ from those of their monomer analogs in solution. Several factors contribute to these differences, including (*a*) a low dielectric permittivity of an adjacent hydrocarbon region, (*b*) fewer degrees of freedom for the immobilized species, (*c*) an excess electrostatic free energy of the supporting surface, and (*d*) changes in the solution dielectric constant in the vicinity of a charged surface (104).

The surface free energy depends on the ionization state of functional groups and reflects their degree of ionization. In principle, one can monitor this change in free energy by measuring contact angle versus pH: There is a large change in contact angle of the buffered droplet at a pH equal to the pK of the surface group (105). Chemically modified AFM tips and samples can be used to probe directly the changes in solid-liquid surface free energies with pH. The surface charge induced by the dissociation of acidic and basic groups can be detected by monitoring the adhesive force with an AFM probe sensitive to electrostatic interactions. Variations in the sign and magnitude of the force will indicate changes in the surface charge, and an abrupt transition will occur at a pH $\approx$ pK of the functional group on the surface.

ADHESION FORCE AND CONTACT ANGLE TITRATIONS Adhesion force values obtained at different solution pHs for tips and samples functionalized with aminopropyltriethoxysilane (APTES) SAMs terminating with amine groups show a sharp drop to zero (indicating a repulsive interaction) below a pH of 4 (Figure 8*A*). The decrease and elimination of an attractive force between the tip and sample is consistent with protonation of the amine groups on these two surfaces. Contact angle values measured using buffered solution droplets on this same surface (Figure 8*B*) also show a sharp transition (an increase in wetability) as the droplet pH is reduced below 4.5. An increase in wetability is expected when the surface becomes protonated. Hence, local force microscopy measurements using a modified probe tip and macroscopic wetting studies provide similar values for the pK of the surface amine groups in the APTES-derived SAMs. The AFM approach to determining local pKs has been termed force titration (34).

The apparent pKs obtained from force microscopy (3.9) and contact angle wetting (4.3) for the surface amine group are 6–7 pK units lower than

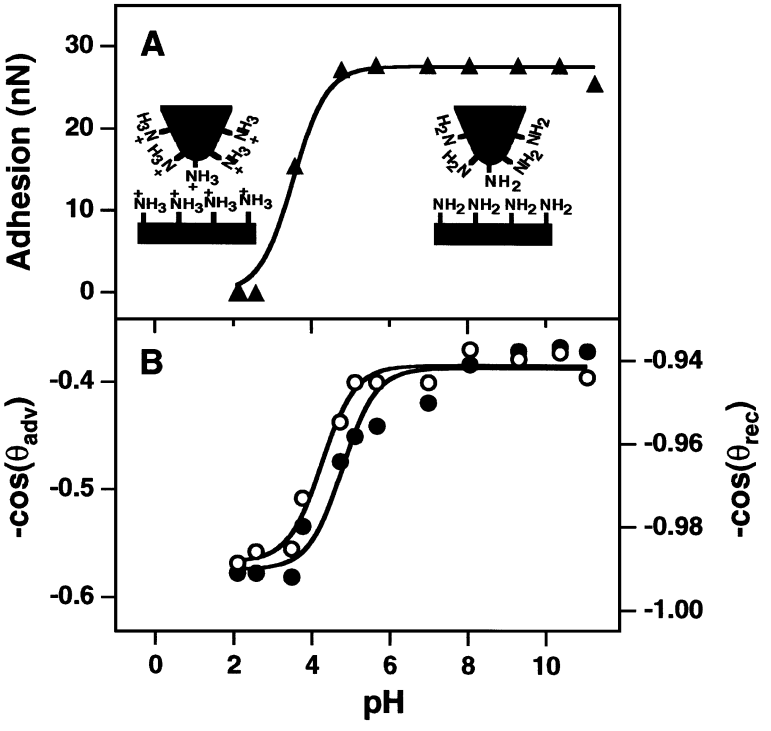

Figure 8 (*A*) Adhesion force between sample and tip functionalized with amino groups versus pH. (*B*) Negative cosines of the advancing (○) and receding (●) contact angles of phosphate buffer droplets on a sample modified with APTES as a function of pH (reproduced from Reference 34).

bulk solution values (100). Large shifts in dissociation constants observed for mixed acid–methyl monolayers were attributed to unfavorable solvation of the carboxylate anion at the monolayer interface (106). Large pK shifts relative to solution were also observed in studies of amino groups grafted onto the surface of a hydrophobic polymer (107). In addition, recent simulations of the titration of surface amine groups showed large negative shifts in pK when the amine was poorly solvated (108). Since the interfacial tension in the alkylamine-water system is almost negligible (<0.1 mJ/m^2) (109), the relatively high contact angles and large adhesion forces at pH > 4 observed in AFM experiments indicate that the APTES-derived monolayers are relatively hydrophobic. The hydrophobic nature of the SAM likely arises from a partially disordered structure that exposes methylene groups at the surface. Hence, the large observed pK shift may be attributed to a hydrophobic environment surrounding the amine groups.

The ability to detect such pK changes locally by AFM should be of significant utility in studies of biological and polymeric systems.

FORCE TITRATIONS ON HYDROPHILIC SURFACES The contact angle technique is limited to surfaces sufficiently hydrophobic that they are not wet completely in either nonionized or ionized states. In the case of high free energy surfaces, such as COOH-terminated SAMs, it is necessary to dilute the hydrophilic groups with a hydrophobic surface component and either pretreat the surface (106) or perform a contact angle experiment under a liquid (versus vapor phase) (110). As our results on the APTES system demonstrate, the incorporation of a hydrophobic component must be done with considerable caution, since it can produce very large pK shifts. Such shifts in the pK_a of surface COOH relative to bulk solution have been observed in cases of mixed COOH and CH_3 SAMs (106, 110). As a result, it has not been possible to determine the pK of a homogeneous COOH-terminated surface using the contact angle approach.

Force titrations provide a direct measure of the solid-liquid interfacial free energy and thus bypass the above-mentioned limitations. A force titration curve obtained for a COOH-terminated sample and tip is shown in Figure 9*A*. A prominent feature in this plot is the sharp transition from positive adhesion forces at low pH to zero (indicating repulsion) at high pH. The observed repulsion at $pH > 6$ can be attributed to electrostatic repulsion between negatively charged carboxylate groups, while the adhesive interaction at low pH values originates from hydrogen bonding between uncharged COOH groups. The force-versus-separation curves become fully reversible and practically identical at all pH values higher than 7, indicating that the surface charge density is saturated under these conditions. Based on these data, we estimate that the pK_a of the surface-confined carboxylic acid is 5.5 ± 0.5. This value lies within 0.75 pK units of the pK_a for COOH functionality in aqueous solution (100). The similarity of surface-confined and solution pK_as indicates strongly that solvation effects do not play a significant role in determining the ionization behavior of pure COOH-terminated SAMs.

Control experiments with both hydrophilic and hydrophobic groups that do not dissociate in aqueous solutions do not display pH-dependent transitions. CFM titration curves for tip/sample SAMs terminating in OH/OH and CH_3/CH_3 functionalities show an approximately constant, finite adhesive interaction throughout the whole pH range studied (Figure 9*B*). The measured adhesion forces between CH_3-terminated SAMs are typically 1–2 orders of magnitude larger than the forces observed for hydrophilic groups (COOH and OH). This large difference shows the importance of hydrophobic forces in aqueous media and supports our conclusion that solvation effects are responsible for the

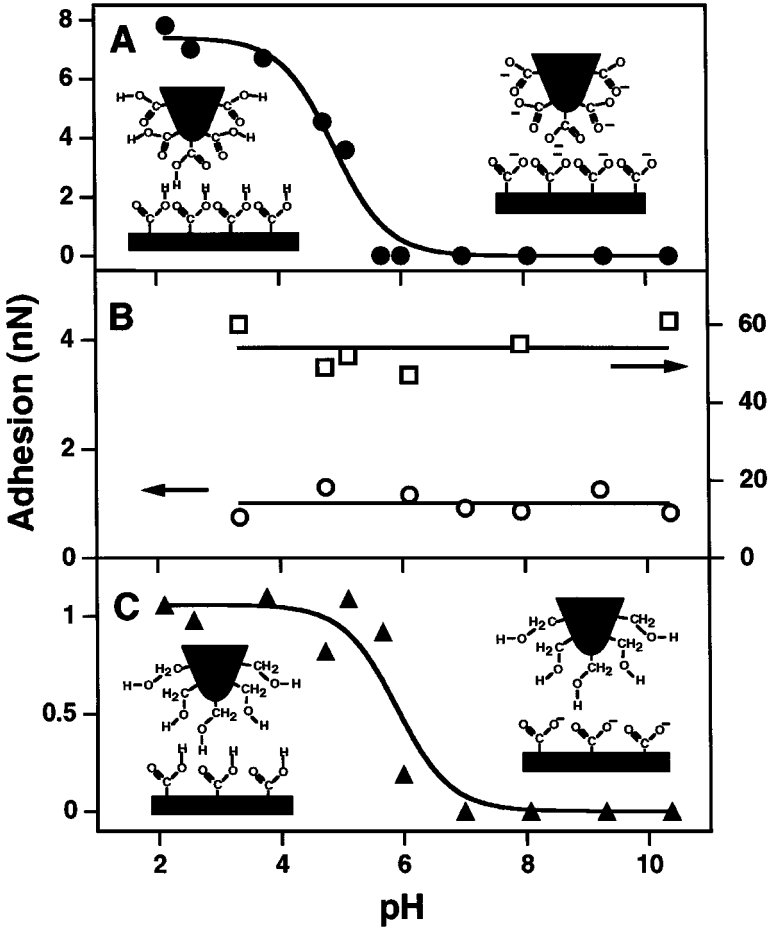

Figure 9 Adhesion force titration curves recorded in buffered solutions. Adhesion force versus pH for (*A*) COOH-COOH, (*B*) CH_3-CH_3 (□) and OH-OH (○), and (*C*) COOH-OH contacts (reproduced from Reference 34).

anomalously high adhesion force (and large shift in pK) between the APTES monolayers.

Finally, to probe pKs on unknown surfaces we suggest the use of functionalized tips with SAMs that (*a*) do not exhibit a pH-dependent change in ionization and (*b*) are hydrophilic. The hydroxyl-terminated SAM meets these requirements and has been used to determine the pK_a of the carboxyl-terminated SAM, as shown in Figure 9*C*. The dissociation constant is within 0.5 pK units of that determined using COOH-terminated SAMs on both sample and tip (Figure 9*A*). The slightly higher pK value is expected because the same magnitude of the

repulsive force is achieved at lower surface charge (lower pH) in the case of overlapping double layers (COOH-COOH) than in the case of a double layer interacting with a neutral, low-dielectric constant surface (COOH-OH).

MODELING THE CHARGED INTERFACE The JKR theory of contact mechanics provides a reasonable basis for understanding adhesion data in aqueous media. To interpret pH-dependent adhesion data in electrolyte solutions, one should also consider long-range electrostatic forces between the tip and sample surfaces. Since the JKR theory is based on energy balance, one expects no adhesion (Hertzian behavior) when the free energy of a double layer per unit area w_{DL} balances γ_{SL}. Quantitatively, the pull-off force, $P_{pull\text{-}off}$, is related to these two terms:

$$P_{pull\text{-}off} = -\frac{3}{2}\pi R W_{SLS} + \frac{5}{2}P_{DL}, \qquad 10.$$

where $P_{DL} \approx 2\pi R w_{DL}$ is an additional load that has to be applied to a spherically shaped tip because of the presence of a double layer. Thus, repulsion between like-charged surfaces ($P_{DL} > 0$) will decrease the magnitude of the pull-off force compared to that given by the JKR theory. There is a threshold value of the repulsive electrical double-layer force $P_{DL} = P_{pull\text{-}off}$, beyond which the deformation of a spherical tip should be fully reversible with a contact radius going monotonically to zero (no pull-off force) as the load is reduced. This result is equivalent to $\gamma_{SL} \approx w_{DL}$. In other words, the attractive surface free energy component is canceled by the repulsive double-layer term. The corresponding surface potential

$$\Psi = \sqrt{\frac{\lambda}{\varepsilon\varepsilon_0}\gamma_{SL}} \qquad 11.$$

is independent of the tip radius for $\lambda \ll R$ (λ is the Debye length). Therefore, the change from adhesive to repulsive behavior is characteristic of the ionization state of the interacting surfaces and can be used to estimate the surface potential.

From the above model, the surface free energies and surface potentials of hydrophilic SAMs can be calculated. The values of γ_{SL} determined from adhesion data for OH- and COOH-(fully protonated) terminated surfaces were 8 $\pm$ 3 mJ/m^2 and 16 $\pm$ 4 mJ/m^2, respectively. These values agree well with the values determined from interfacial tension measurements using two-phase systems consisting of water and melts of either long-chain alcohols (7–8 mJ/m^2) (111) or carboxylic acids (10–11 mJ/m^2) (112). The surface potential of the carboxylate SAM at pH > 6 and IS $= 0.01$ M, -140 ± 20 mV, calculated from Equation 11, is in reasonable agreement with an independent analysis of long-chain, fatty-acid monolayers at the air-water interface under the same condition (113). This result can be substantiated further by analysis of F-D curves as discussed below.

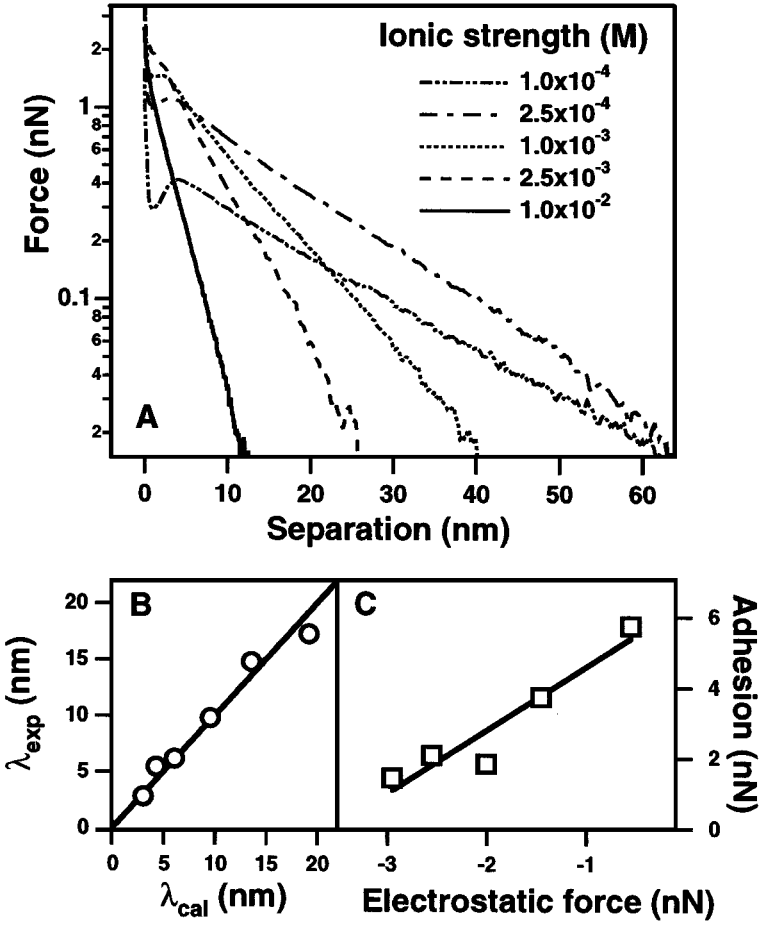

Figure 10 (*A*) Repulsive double-layer force versus separation recorded upon approach between COOH-modified tips and samples at different solution ionic strengths at pH = 7.2. (*B*) Debye length obtained from experimental data in (*A*) and calculated from solution ionic strength. (*C*) Observed relationship between the adhesion force and repulsive electrostatic force, $-(-P_{DL})$, for COOH-terminated tips and samples (reproduced from Reference 34).

PROBING DOUBLE-LAYER FORCES The electrostatic origin of the pH-dependent repulsive forces can be verified by changing the Debye screening length λ, that is, the solution ionic strength. Figure 10*A* shows that the repulsive interaction becomes progressively longer-ranged as the solution ionic strength, IS, decreases. A detailed analysis of the electrostatic force requires consideration of the surface charge–potential regulation imposed by the potential-dependent

binding of H^+ and Na^+ ions at the interface. Surface charge–potential regulation has been observed in colloidal probe microscopy investigations (114, 115), and this concept has been used in SFA studies to analyze double-layer interactions involving mica surfaces and 1:1 electrolytes (62).

Data in Figure 10*A* were analyzed with a model that uses a linearized charge-potential regulation condition (116). For carboxylate surfaces, the experimental data (IS = 0.01 M) was well-fit down to separations of 1 nm. The condition of constant charge (versus constant potential) was approached in these experiments independent of ionic strength. The values of the screening length, λ_{exp}, extracted from experimental F-D curves agree well with the values calculated from the solution ionic strengths, λ_{cal} (Figure 10*B*). Significantly, the surface potential calculated using this analysis of the COOH-terminated surface at pH = 7.2 and 0.01 M ionic strength (-120 ± 5 mV) is close to the value estimated from adhesion measurements. It may be possible to determine double-layer parameters of systems being imaged by simultaneously recording F-D curves, using a tip bearing a functional group with a predetermined ionization behavior.

Figure 10*A* also shows that the magnitude of the electrostatic force decreases for IS $< 1 \times 10^{-2}$ M at small tip-sample separations. Equivalently, the values of P_{DL} determined from the above fits decrease for IS $< 1 \times 10^{-2}$ M. In addition, adhesion can occur between surfaces despite the repulsive interaction. A plot of the measured adhesion force as a function of the electrostatic force, $-P_{DL}$, is shown in Figure 10*C*. This phenomenon is fully reversible: By varying the ionic strength one can go from pure repulsion at high ionic strengths to repulsion on approach and adhesion on separation at low ionic strengths. A decrease in ionic strength (larger λ) will diminish the double-layer repulsion (Figure 10*A*), which according to Equation 10 should result in a larger adhesion force as found in Figure 10*C*.

Finally, the number of species involved in double-layer interactions can be estimated. For a tip with a radius of 30 nm in contact with the sample surface in solution of 0.01 M ionic strength, more than 200 ions and 1×10^5 water molecules are involved in the interaction. This observation contrasts the situation in organic solvents where there are typically only 15–25 molecular contacts (33). Thus, when using repulsive electrostatic forces in constant force imaging, one must remember that these forces are averaged over relatively large sample areas (117–119).

FRICTION MEASUREMENTS

We (8, 33, 34) and others (42) have observed that microscopic friction and adhesive forces correlate with each other for organic monolayer systems. The friction force between functional groups on a sample surface and tip is usually

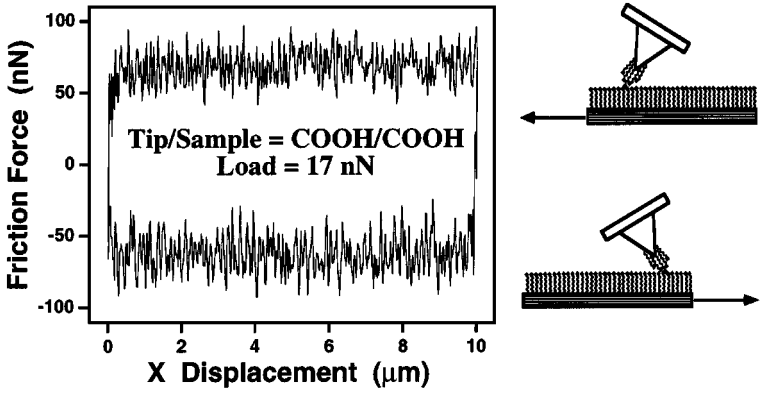

Figure 11 A typical friction loop recorded on a COOH-terminated sample using a COOH-modified tip in EtOH solution (adapted from Reference 33).

determined by recording the lateral deflection of the cantilever as the sample is scanned in a forward-backward cycle along the direction perpendicular to the cantilever axis to produce a friction loop (120) (Figure 11). The externally applied load is controlled independently through the cantilever normal deflection. The numerical values of the normal and lateral forces are determined using the cantilever spring constants, and friction coefficients are obtained from the slopes of the corresponding friction-versus-load (F-L) curves. Another approach that utilizes a two-dimensional histogramming technique to produce F-L curves has also been proposed (75, 121–123).

Chemical Effects in Friction

In ambient conditions, it is difficult to distinguish from other factors the true chemical contributions to friction. First, the large magnitude of capillary adhesion can produce normal loads drastically higher than the externally applied load. This increase in load results in large increases in contact areas and hence friction forces (122). Second, films of condensed vapor on surfaces can act as boundary lubricants and reduce friction between the surface and the AFM probe (122, 124). Both effects obscure true chemical interactions and can be eliminated by performing measurements either in liquids or ultrahigh vacuum. In addition, the generally uncontrolled surface functionality of Si and Si_3N_4 tips (i.e. SiOH density and varying degrees of contamination with hydrocarbons) indicates that well-defined, modified tips are also needed to assess true chemical contributions to friction.

Friction forces between tips and samples modified with different functional groups have been measured in ethanol (33), water (34), and dry argon (42) as a

Table 3 Frictional forces between functional groups

No.	Functional group pair (tip-sample)	Monolayer, chain length	Medium	Friction coefficient	Ref.	Tip radius (nm)
1	COOH-COOH	thiol, C_{16}	dry Ar	1.0	42	NR (20–40)[a]
2	COOH-CH_3	thiol, C_{16}, C_{18}	dry Ar	$\approx$0	42	NR (20–40)[a]
3	CH_3-COOH	thiol, C_{18}, C_{16}	dry Ar	0.03	42	NR (20–40)[a]
4	CH_3-CH_3	thiol, C_{18}	dry Ar	0.07	42	NR (20–40)[a]
5	COOH-COOH	thiol, C_{11}	EtOH	2.5	33	60
6	COOH-CH_3	thiol, C_{11}, C_{18}	EtOH	0.4	33	60
7	CH_3-CH_3	thiol, C_{18}	EtOH	0.8	33	60
8	CH_3-CH_3	thiol, C_{18}	H_2O[b]	0.3	34	30
9	COOH-COOH	thiol, C_{11}	H_2O, pH < 5[b]	1.9	34	40
10	COOH-COOH	thiol, C_{11}	H_2O, pH > 7[b]	0.4	34	40
11	COOH-CH_2OH	thiol, C_{11}	H_2O, pH < 5[b]	1.0	34	40
12	COOH-CH_2OH	thiol, C_{11}	H_2O, pH > 7[b]	0.5	34	40
13	CH_2OH-CH_2OH	thiol, C_{11}	H_2O[b]	0.3	34	40

[a]Tips were coated with 40 nm of Au.
[b]Ionic strength IS $=$ 0.01 M.

function of an applied load (Table 3). In these measurements, the friction forces increased linearly with the applied load. For a fixed external load the absolute friction force decreased as COOH/COOH $>$ CH_3/CH_3 $>$ COOH/CH_3 (33, 42), as shown in Figure 12. The trend in the magnitude of friction forces and friction coefficients is the same as that observed for the adhesion forces: COOH/COOH-terminated tips and samples yield large friction and adhesion forces, while the COOH/CH_3 combination displays the lowest friction and adhesion. Thus a direct correlation exists between the friction and adhesion forces measured between well-defined SAM surfaces. SFA studies of structurally similar layers also show that the friction force correlates with the force of adhesion (125). In contrast, a better correlation with adhesion hysteresis and not the adhesion force was found in SFA studies of dissimilar phases (i.e. crystalline, amorphous, and liquid-like) of different hydrocarbon surfactants (15–18).

SINGLE ASPERITY CONTACTS The JKR model used to interpret the adhesion data predicts nonlinear dependence for friction versus load when a single spherical tip contacts a planar surface. Nonlinear behavior should be detectable in systems that exhibit a large adhesion, such as hydrophobic SAMs in water, at small or tensile loads. F-L data acquired for CH_3-terminated SAMs in water (Figure 13) show nonlinear dependence on applied load and are well-fit to the contact area-vs-load dependence predicted by the JKR model (92). These results demonstrate that CFM probes the friction arising from interactions within a single asperity contact. This type of contact has also been reported for Si_3N_4

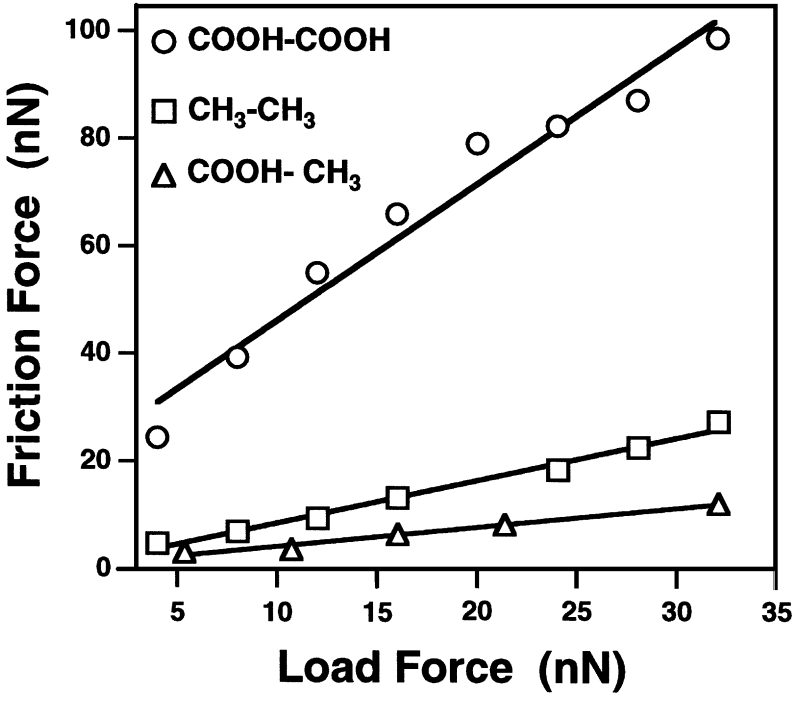

Figure 12 Summary of the friction force-versus-applied load data recorded for functionalized samples and tips terminating in COOH/COOH (○), CH_3/CH_3 (□), and $COOH/CH_3$ (△) in EtOH (reproduced from Reference 33).

tips on mica (79) and siloxane-coated mica (126), for monolayers of C_{60} on GeS (127), for Si tips on NaCl (121), and for Pt-coated tips on mica (128, 129).

IONIZABLE SURFACE GROUPS The change in ionization state of functional groups can also be detected by recording frictional forces at different pH. F-L curves for COOH-terminated tips and samples are linear but fall into two distinct categories: Larger friction forces and friction coefficients are found in solutions at pH $<$ 6 compared to pH $>$ 6 (Figure 14). This cross-over in behavior occurs at the same region of pH where the normal forces exhibit a transition from attraction to repulsion. A finite load ($\sim$4 nN) is necessary to achieve nonzero friction at high pH. This is the load required to overcome the double-layer repulsion (between charged surfaces) and bring the tip into physical contact with the sample surface. Similar pH-dependent friction forces were reported for Si_3N_4 tips on Si surfaces and were attributed to protonation-

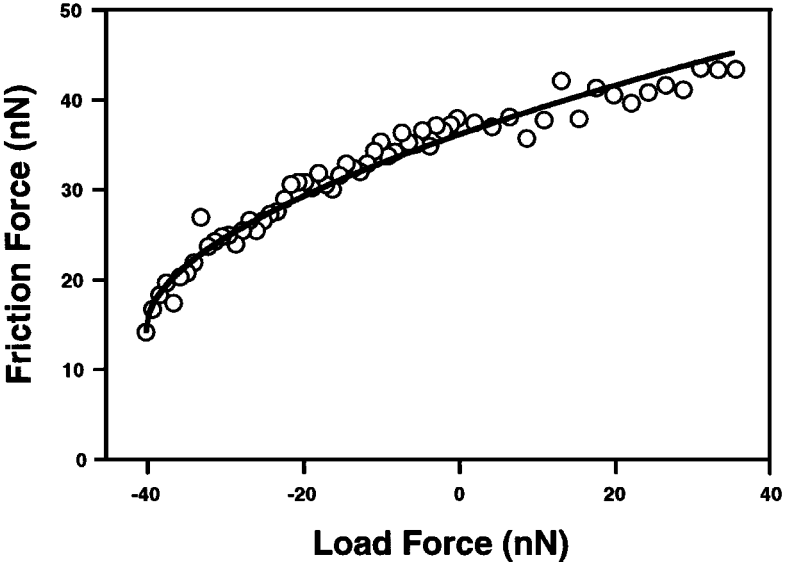

Figure 13 Friction force-versus-applied load curve (○) for a CH_3-terminated tip and sample in water. The concave shape of the curve is consistent with the nonlinear dependence of the contact area on external load predicted by the JKR model (—).

deprotonation of tip/sample SiOH groups (130). Although this hypothesis is reasonable, we believe that the acid-base behavior of the SAMs is much better defined and hence amenable to more detailed understanding (e.g. the isoelectric point for SiOH groups is expected to be around $pH = 2$, whereas the transition in friction force occurs near $pH = 6$).

The frictional behavior of tips and samples functionalized with ionizable and nonionizable SAMs can be summarized in plots of the friction coefficient versus pH (Figure 15). The friction coefficients determined for OH- and CH_3-terminated SAMs (not shown) are independent of pH, as expected for neutral, nonionizable functional groups. In contrast, the friction coefficients determined for cases in which one or both SAM surfaces terminate in carboxyl groups show significant decreases at pH above the pK_a of the surface COOH group. The friction coefficients thus exhibit similar pH dependencies to those observed in adhesion measurements. These results suggest that the drop in friction coefficient with changes in pH can be associated with the ionization of surface groups.

We also found that the magnitudes of the friction force and friction coefficient for OH-terminated surfaces were the lowest of those investigated in aqueous

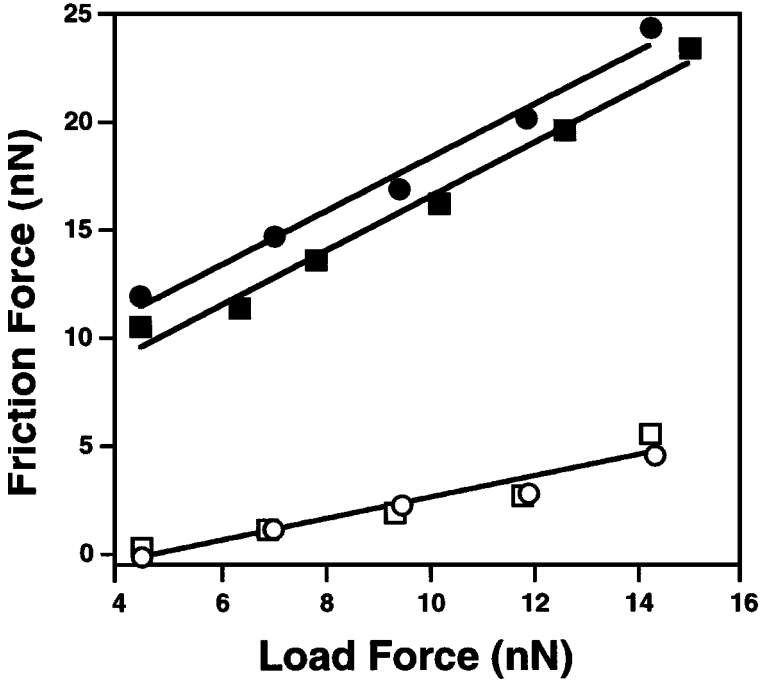

Figure 14 Friction force versus applied load curves for COOH-COOH functionalized samples and tips recorded at pH 2.2 (●), 3.5 (■), 7.0 (○) and 9.3 (□) (reproduced from Reference 34).

solution. Analysis of F-L curves for CH_3-terminated tip/sample combinations also yielded low friction coefficients (∼0.3); however, for comparable tip radii the magnitude of the friction force was an order of magnitude greater (∼60 nN) than for either COOH or OH functionalized surfaces. The large magnitude of the friction force between CH_3 surfaces in aqueous media originates from the large contact area between hydrophobic surfaces.

Mechanical Properties of the SAMs

Other monolayer properties can affect adhesive and frictional behavior of organic layers. For example, studies of phase-segregated Langmuir-Blodgett films have indicated that elasticity and crystallinity correlate with observed friction (131) and adhesion (132). A chain-length dependence was observed for friction on silane SAMs on mica (126) and LB films of saturated carboxylic acids (133). This chain-length dependence may reflect structural differences in the various monolayers versus an intrinsic viscoelastic effect (126). Our studies of adhesion between samples that have been modified with different

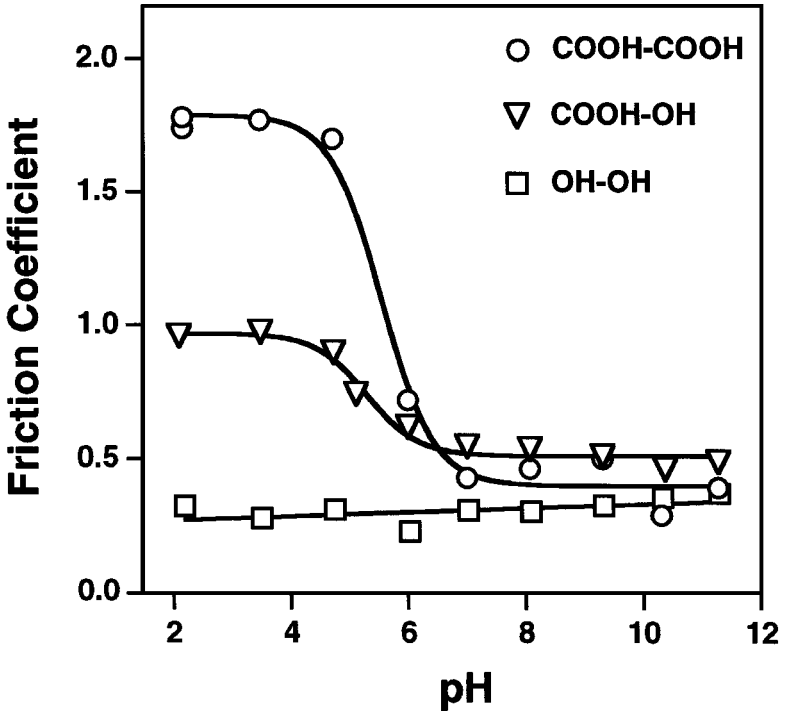

Figure 15 Friction coefficient versus pH for COOH-COOH (○), COOH-OH (▽), and OH-OH (□) contacts (reproduced from Reference 34).

chain-length SAMs, $HS(CH_2)_nCH_3$ ($n = 11, 51, 21, 25$) and tips modified with a single $n = 15$ SAM in methanol show only small differences as a function of chain length (tip R $\approx$ 20 nm): 0.53 ± 0.16 ($n = 11$), 0.57 ± 0.16 ($n = 15$), 0.47 ± 0.13 ($n = 21$) and 0.45 ± 0.12 nN ($n = 25$). As a result, we believe that chemical effects dominate observed adhesive and frictional differences in structurally well-defined systems.

CHEMICALLY SENSITIVE IMAGING

Achieving chemical sensitivity in scanning probe microscopy imaging has been a goal since the technique's invention. Sensitivity to the surface composition combined with unparalleled resolution and the ability to image a diverse array of surfaces under a variety of conditions would make AFM an even more powerful scientific tool; however, several key issues regarding this problem must be addressed. The contrast in AFM images originates from the interactions

between the probe tip and the surface. These interactions are dependent on surface chemistry, morphology, mechanical properties, and on the nature of the surrounding medium. In order for chemical contrast to dominate observed images, chemically specific forces must be identified and enhanced, and other forces reduced or eliminated. Once the origin of the chemical contrast is understood, one can envision fine-tuning the probe-surface interactions as a way of enhancing the imaging sensitivity and specificity.

Lateral Force Imaging

The results presented above show that chemical modification of probe tips is often sufficient to observe chemical sensitivity in normal and lateral forces. The observed differences in friction can be exploited to produce lateral force images of heterogeneous surfaces with predictable contrast (8, 33, 34, 42). Patterned SAMs of alkane thiols on Au surfaces present a convenient model system for such studies because they are readily prepared, can incorporate a variety of different terminal functionalities, and have similar mechanical properties regardless of the terminal functional group. In addition, patterned surfaces can be made relatively flat, thus eliminating unwanted topographic contributions to lateral force images.

Figure 16*A* shows a topographical image of a photochemically patterned SAM (134) with 10 μm $\times$ 10 μm square regions that terminate with COOH groups and repeat every 30 μm in a regular pattern. The regions of the SAM surrounding these squares terminate with CH_3 groups. Topographical images failed to reveal this pattern since such surfaces exhibit almost flat topography across the CH_3- and COOH-terminated regions of the sample. Friction maps of these samples taken with different tip functionality readily show chemical information about the surfaces (Figure 16*B*, *C*). Friction maps recorded with COOH tips display high friction on the area of the sample that terminates in COOH groups, and low friction on the CH_3-terminated regions. Images recorded with CH_3 tips exhibit a reversal in the friction contrast: Low friction is found in the area of the sample that contains the COOH-terminated SAM, and higher friction is observed in the surrounding CH_3 regions.

As expected, this reversal in friction contrast is consistent with the F-L curves obtained on homogenous SAM samples and occurs only with changes in the probe tip functionality. The image resolution is not that of a single functional group but rather an ensemble of groups defined by the tip contact area. Moreover, in the images shown in Figure 16, the resolution is limited by the photopatterning method itself ($\sim$200 nm). Employing a microcontact printing technique for pattern generation improves the resolution by a factor of 4–5 (50). In addition, a resolution on the order of 10–20 nm was achieved in a monolayer-bilayer $COOH/CH_3$ system with functionalized tips in dry argon atmosphere (42).

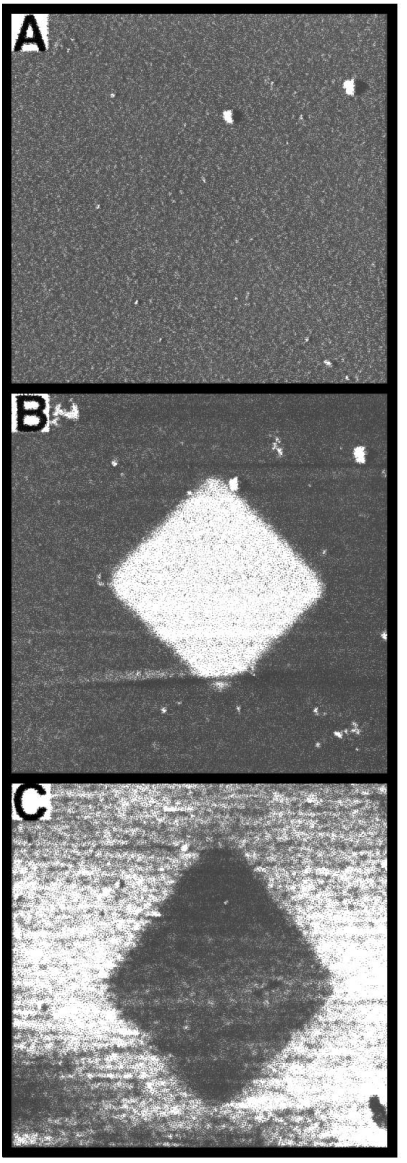

Figure 16 Force microscopy images of a photopatterned SAM sample. The 10×10 μm square region terminates in COOH, and the surrounding region terminates in CH_3. The images are of (*A*) topography, (*B*) friction force using a tip modified with a COOH-terminated SAM, and (*C*) friction force using a tip modified with a CH_3-terminated SAM. Light regions in (*B*) and (*C*) indicate high friction; dark regions indicate low friction (reproduced from Reference 33).

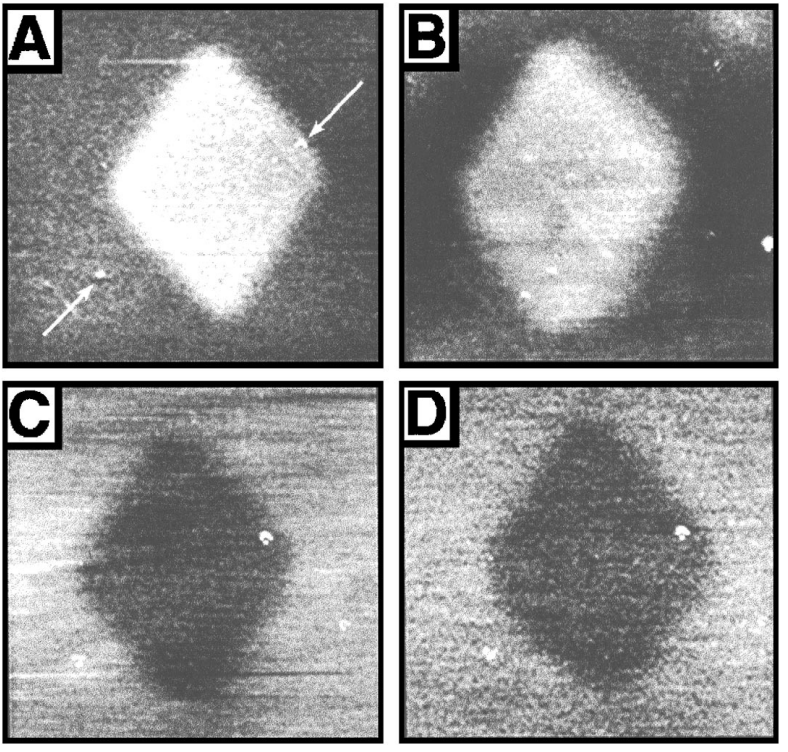

Figure 17 Lateral force images of the same region of a patterned SAM sample in which the inner square terminates with COOH groups and the surrounding background with OH groups. The images were recorded with pH values of (*A*) 2.2, (*B*) 4.8, (*C*) 7.2, and (*D*) 10.3. Two particles are highlighted by arrows on image A and also can be seen in images C and D. Image size is (30 μm $\times$ 30 μm). Light regions indicate high friction; dark regions indicate low friction.

A general approach for enhancing chemical sensitivity involves changing the solvent characteristics, such as composition (44) or pH (34). The validity of this approach was demonstrated by mapping changes in functional group ionization states with varying solution pH values. Images of COOH/OH-patterned surfaces obtained with a COOH-terminated tip in different pH solutions show that the friction contrast between COOH/OH regions can be inverted reversibly and that the change in contrast occurs near the pK_a of the surface carboxyl (Figure 17).

The reversals in friction contrast presented above occur only with changes in the probe tip functionality or a change in the probe tip ionization state in both ethanol and aqueous solvents. These results demonstrate the chemical-sensitive imaging possible with specifically functionalized tips that we term chemical

force microscopy (CFM). The approach is reproducible and may serve as a method for mapping more complex and chemically heterogeneous surfaces. Chemically modified tips have also been used in imaging patterned siloxane monolayers on Si (135) and single polymers adsorbed on latex spheres (136). These reports claimed to achieve pseudo-height contrast dependent on the AFM tip functionality; however, this contrast should be interpreted as a friction image with the tip scanned parallel to the cantilever axis of symmetry (70, 137).

OTHER CONSIDERATIONS Differences in friction forces have been used to map different domains of phase-segregated LB films (131). The image contrast in these investigations, however, was believed to result from differences in the elastic properties of the domains and not from the chemical functionality at the film surface. In systems where elasto-mechanical effects (or differences resulting from them) are eliminated, the chemical component of the tip-surface interaction can be the dominant one determining observed image contrast. Conversely, if the interfacial chemistry is the same, second-order effects (e.g. elasto-mechanical) can become dominant (133).

The conditions under which the imaging is performed are important, since dominant interactions depend on the media even for the same tip-surface system. Figure 18 shows lateral force images of a $COOH/CH_3$ pattern acquired in water and air using a CH_3-functionalized tip. The friction contrast between COOH and CH_3 functional groups is relatively large in both images. In water, this pattern shows high friction on the CH_3-terminated regions and low friction over the COOH-terminated regions of the sample. This result is readily understood on the basis of the friction studies discussed above. The contrast reflects the dominant effect of hydrophobic forces that mask other chemical interactions. Thus imaging under water with hydrophobic CH_3-terminated tips constitutes an approach to construct hydrophobicity maps of sample surfaces such as biomedical polymers.

Images acquired in air exhibit friction contrast opposite to that obtained in aqueous solution. These images do not reflect chemical interactions directly, but rather are the result of large capillary forces between the sample and tip over the hydrophilic COOH-terminated areas of the surface that are wet more readily than CH_3 regions. The high friction on the hydrophilic patches of the surface is always observed in air regardless of whether the tip is bare Si_3N_4 (50) coated with Au, or derivatized with COOH or CH_3 functional groups (33). Although chemical modification of the tips does not influence the contrast controlled by capillary forces, it can reduce the contact forces and thereby enhance imaging resolution. In fact, hydrophobic treatment of AFM probes to reduce capillary forces and enhance the image resolution is a well-known trick in the AFM community (44, 48, 138).

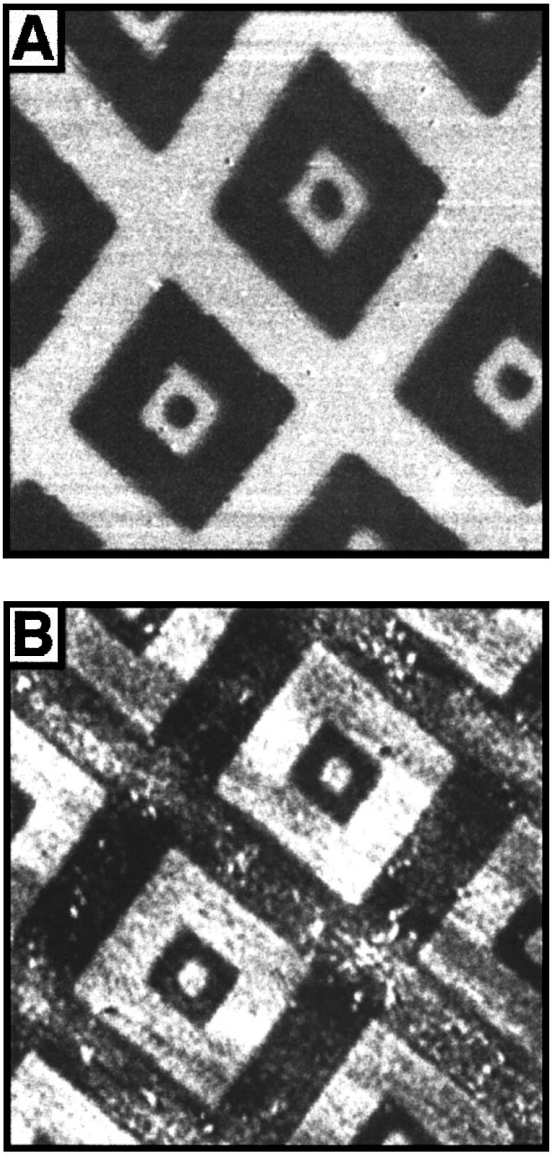

Figure 18 Lateral force image of a sample patterned with regions terminating in CH_3 and COOH functional groups recorded in (*A*) DI water and (*B*) air with a methyl-functionalized tip. (*A*) Light regions are areas of high friction and correspond to surface regions terminating in CH_3 functionality. Dark regions represent low friction and correspond to the surface areas terminating in COOH functional groups. (*B*) The high friction (light) areas correspond to regions terminating in COOH groups, while the low friction (dark) areas correspond to the CH_3-terminated regions. The images are 100 μm $\times$ 100 μm.

Other Modes of Imaging

Considerable attention has been directed toward the development and understanding of resonance imaging techniques. The tapping mode AFM (139) method has achieved the greatest popularity. In tapping mode, a tip is vibrated near the surface, so that it briefly touches the surface on each oscillation. Changes in the oscillation amplitude are monitored by the feedback loop as the sample is rastered under the probe tip. Advantages of tapping mode over conventional contact mode are that (*a*) the tip-sample forces act on a shorter time scale and (*b*) lateral forces are almost completely eliminated. These advantages, combined with the tapping mode's ability to image in physiologically relevant media (140), make it a suitable method for imaging soft polymer surfaces and biological samples. In fact, tapping mode has been used successfully in imaging etched polymers (141), cell surfaces (142), microtubules (143), chromatin fibers (144), proteins (145), and DNA (146). Phase detection in tapping mode (147) can also yield very high-resolution images. Phase detection involves measuring the phase lag between the drive signal and tip response.

One can envision that bringing our CFM approach to tapping mode would enable nondestructive chemical mapping of delicate samples. Chemically heterogeneous surfaces produced by microcontact printing of alkanethiols on Au are good model substrates for these studies (50). Since they are prepared using thiols of equal lengths that differ only in the functionality of the terminal carbon, the samples are essentially flat and the regions of different chemical functionality are expected to have similar elastic properties. Therefore, most of the structural differences that can contribute to the contrast in the images are eliminated.

Figure 19*B* shows a tapping-mode phase image obtained with a COOH-terminated tip on a microstamped sample bearing a uniform box-within-a-box pattern of alternating methyl and carboxyl groups. The regions of different chemical composition are readily identifiable on the image, showing that phase-lag imaging is sensitive to differences in tip-sample interactions. Phase-image contrast correlates with that in the friction image of the same sample obtained with the same tip (Figure 19*A*): Light areas on friction images are dark areas on phase images (i.e. greater friction and greater phase lag occur in the same regions). We have proposed that the phase contrast observed with soft cantilevers in liquids can be attributed in certain cases to differences in adhesion forces (A Noy, CH Sanders, SS Wong, DV Vezenov, CM Lieber, unpublished results).

When the tip functionality was switched to methyl, the phase-image contrast inverted (Figure 19*C*). Moreover, when the medium was changed from ethanol to water the magnitude of the phase lag increased several fold, whereas no contrast reversal took place upon varying tip functionality. These latter results are also consistent with the adhesion-friction data discussed above. This

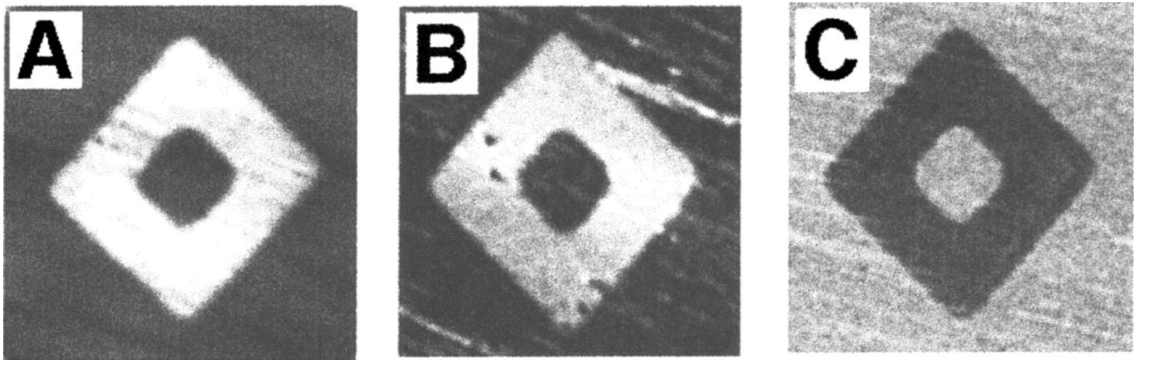

Figure 19 Force microscopy images of a CH_3-terminated square in a COOH square surrounded by a CH_3 SAM pattern prepared by microcontact printing. The images are recorded in ethanol and represent (*A*) a friction map recorded with a tip modified with a COOH-terminated SAM, (*B*) a phase lag map acquired with a tip modified with a CH_3-terminated SAM, and (*C*) a phase lag map acquired with a tip terminating in COOH groups. Light areas in (*A*) indicate higher friction; dark regions in (*B*) and (*C*) indicate greater phase lag. Image sizes are 20 μm $\times$ 20 μm.

observation shows that phase-lag imaging is highly sensitive to the nature of the chemical interactions between the sample surface and the probe: Regions that interact more strongly produce greater phase lag (darker areas), whereas regions with weaker interactions produce smaller phase lag (lighter areas). These results demonstrate the potential of tapping mode for mapping functional group distributions in a predictable way.

CONCLUSIONS

Chemically modified tips produced by covalently linking molecules to force microscope probe tips may be used to measure and quantify adhesion and friction forces between the functional groups on a tip and sample. Adhesion studies between SAMs that terminate with hydrogen bonding and hydrophobic functional groups have shown that the interaction between these groups follows chemical intuition and can be interpreted using a surface tension component model. These adhesion forces agree well with forces predicted by the JKR theory of adhesive contact. This model also makes it possible to show that the contact area between sharp ($<$50 nm) tips and the sample corresponds to an interaction between only 15–25 molecular pairs in organic solvent media, although the number of interacting species for charged surfaces in water is an order of magnitude greater. Analyses of available CFM data show that it is possible to determine surface free energies for organic surface-liquid and surface–inert gas interfaces, as well as solid-solid interfacial free energies that are not readily obtainable by contact angle measurements. A new method has also been developed to determine local pKs of surface ionizable functional groups through force titrations. The interactions observed between modified tip and sample surfaces in aqueous solutions also agree well with the predictions of double-layer and modified JKR models. These models have been used to extract surface free energies and double-layer parameters that are essential to understanding interactions in aqueous media.

In addition, the friction forces between modified tips and samples were found to be chemically specific. The magnitudes of the friction forces follow the same trend as adhesion forces. Frictional forces between ionizable groups are also dependent on the ionization states of interacting functionalities. Specifically, the friction coefficient for COOH-terminated surfaces decreases significantly at a pH corresponding to the pK_a determined from adhesion measurements. The predictable dependence of friction forces on the tip and sample functionality is the basis for chemical force microscopy, in which lateral force images are interpreted in terms of the strength of adhesive and shear interactions between functional groups. Thus, in conjunction with adhesion data, CFM can distinguish different functional group domains in organic and aqueous solvents.

When present, hydrophobic effects dominate both adhesion and friction forces; hence, lateral force images taken with hydrophobic tips in aqueous solutions can map hydrophobic regions on a sample. On hydrophilic surfaces, observed pH-dependent changes in friction forces of ionizable groups can be used to map surfaces terminating in hydrophilic functional groups and to define the ionization state as a function of pH.

These studies open many opportunities for basic and applied research. A variety of intermolecular interactions can be studied using the CFM technique, and analysis of these data can provide basic thermodynamic information relevant to chemists and biologists. CFM imaging of systems such as polymers, biomolecules, and other materials could lead to new insights into the spatial distribution of functional groups, hydrophobic versus hydrophilic domains, and/or improved resolution. Our approach of using force titrations to determine the local pK of acidic and basic groups may be applicable to probing the local electrostatic properties of protein surfaces in their native environments and the ionization of colloidal particles at the nanoscale. Studies using chemically modified tips should also provide insight into the molecular mechanisms of dissipative processes relevant to tribology.

Literature Cited

1. Bhushan B. 1995. *Handbook of Micro/nanotribology.* Boca Raton: CRC Press
2. Kendall K. 1994. *Science* 263:1720
3. Israelachvili J. 1992. *Intermolecular and Surface Forces.* New York: Academic
4. Creighton TE. 1993. *Proteins: Structure and Molecular Properties.* New York: Freeman
5. Binnig G, Quate CF, Gerber C. 1986. *Phys. Rev. Lett.* 56:930
6. Colton RJ. 1996. *Procedures in Scanning Probe Microscopy.* New York: Wiley & Sons
7. Smith DPE. 1995. *Rev. Sci. Instr.* 66:3191
8. Frisbie CD, Rozsnyai LF, Noy A, Wrighton MS, Lieber CM. 1994. *Science* 265:2071
9. Albrecht TR, Akamine S, Carver TE, Quate CF. 1990. *J. Vac. Sci. Technol. A* 8:3386
10. Meyer G, Amer NM. 1988. *Appl. Phys. Lett.* 53:1045
11. Meyer G, Amer NM. 1990. *Appl. Phys. Lett.* 57:2089
12. Burnham NA, Colton RJ, Pollock HM. 1991. *J. Vac. Sci. Technol. A* 9:2548
13. Joyce SA, Houston JE. 1991. *Rev. Sci. Instr.* 62:710
14. Kato N, Suzuki I, Kikuta H, lwata K. 1995. *Rev. Sci. Instr.* 66:5532
15. Israelachvili J. 1987. *Acc. Chem. Res.* 20:415
16. Yoshizawa H, Chen YL, Israelachvili J. 1993. *J. Phys. Chem.* 97:4128
17. Chen YL, Helm CA, Israelachvili JN. 1991. *J. Phys. Chem.* 95:10736
18. Israelachvili J. 1992. *J. Vac. Sci. Technol. A* 10:2961
19. Chaudhury MK, Whitesides GM. 1991. *Langmuir* 7:1013
20. Chaudhury MK, Whitesides GM. 1992. *Science* 255(5049):1230
21. Ducker WA, Senden TJ, Pashley RM. 1991. *Nature* 353:239
22. Ducker WA, Senden TJ, Pashley RM. 1992. *Langmuir* 8:1831
23. Thomas RC, Houston JE, Crooks RM, Kim T, Michalske TA. 1995. *J. Am. Chem. Soc.* 117:117
24. Ashkin A, Dziedzic JM, Bjorkholm JE,

Chu S. 1986. *Optics Lett.* 11:288
25. Kuo SC, Sheetz MP. 1993. *Science* 260:232
26. Svoboda K, Schmidt CF, Schnapp BJ, Block SM. 1993. *Nature* 365:721
27. Perkins T, Smith DE, Chu S. 1994. *Science* 264:819
28. Finer JT, Simmons RM, Spudich JA. 1994. *Nature* 386:113
29. Johnson SB, Drummond CJ, Scales PJ, Nishimura S. 1995. *Langmuir* 7:2367
30. Tsao Y-K, Evans DF, Wennerström H. 1993. *Science* 262:547
31. Parker JL, Claesson PM. 1992. *Langmuir* 8:757
32. Biggs S, Mulvaney P. 1994. *J. Chem. Phys.* 100:8501
33. Noy A, Frisbie CD, Rosznyai LF, Wrighton MS, Lieber CM. 1995. *J. Am. Chem. Soc.* 117:7943
34. Vezenov DV, Noy A, Rosznyai LF, Lieber CM. 1997. *J. Am. Chem. Soc.* In press
35. Nuzzo RG, Allara DL. 1983. *J. Am. Chem. Soc.* 105:4481
36. Porter MD, Bright TB, Allara DL, Chidsey CED. 1987. *J. Am. Chem. Soc.* 109:3559
37. Bain CD, Troughton EB, Tao Y-T, Evall J, Whitesides GM, et al. 1989. *J. Am. Chem. Soc.* 111:321
38. Bain CD, Evall J, Whitesides GM. 1989. *J. Am. Chem. Soc.* 111:7155
39. Whitesides GM, Laibinis PE. 1990. *Langmuir* 6:87
40. Nakagawa T, Ogawa K, Kurumizawa T, Ozaki S. 1993. *Jpn. J. Appl. Phys.* 32:L294
41. Nakagawa T, Ogawa K, Kurumizawa T. 1994. *J. Vac. Sci. Technol. B* 12:2215
42. Green J-B, McDermott MT, Porter MD, Siperko LM. 1995. *J. Phys. Chem.* 99:10960
43. Thomas RC, Tangyunyong P, Houston JE, Michalske TA, Crooks PM. 1995. *J. Am. Chem. Soc.* 98:4493
44. Sinniah SK, Steel AB, Miller CJ, Reutt-Robey JE. 1996. *J. Am. Chem. Soc.* 118:8925
45. Sharma R, Wood J. 1995. *Langmuir* 11:4797
46. Pierce M, Stuart J, Pungor A, Dryden P, Hlady V. 1994. *Langmuir* 10:3217
47. Thomas RC, Tangyunyong P, Houston JE, Michalske TA, Crooks RM. 1994. *J. Phys. Chem.* 98:4493
48. Alley RL, Komvopoulos K, Howe RT. 1994. *J. Appl. Phys.* 76:5731
49. Grigg DA, Russell PE, Griffith JE. 1992. *J. Vac. Sci. Technol. A* 10:680
50. Wilbur J, Biebuyck HA, MacDonald JC, Whitesides JM. 1995. *Langmuir* 11:825
51. Weisenhorn AL, Hansma PK, Albrecht TR, Quate CF. 1989. *Appl. Phys. Lett.* 54:2651
52. Drake B, Prater CB, Weisenhorn AL, Gould SAC, Albrecht TR, et al. 1989. *Science* 243:1586
53. Vesenka J, Mosher C, Schaus S, Ambrosio L, Henderson E. 1995. *BioTechniques* 19:240
54. Shao Z, Yang J. 1995. *Q. Rev. Biophys.* 28:195
55. Lyubchenco YL, Oden PI, Lampner D, Lindsay SM, Dunker KA. 1993. *Nucleic Acids Res.* 21:1117
56. Weisenhorn AL, Maivald P, Butt HJ, Hansma PK. 1992. *Phys. Rev. B* 45:11226
57. Butt HJ. 1991. *Biophys. J.* 60:1438
58. van der Werf KO, Putman CAJ, de Grooth RG, Greve J. 1994. *Appl. Phys. Lett.* 65:1195
59. Ishino T, Hieda H, Tanaka K, Gemma N. 1994. *Jpn. J. Appl. Phys.* 33:4718
60. Johnson SB, Drummond CJ, Nishimura S. 1995. *Langmuir* 11:2367
61. Vigil G, Xu Z, Steinberg S, Israelachvili J. 1994. *J. Colloid Interface Sci.* 165:367
62. Pashley RM. 1981. *J. Colloid Interface Sci.* 83:531
63. Xu S, Arnsdorf MF. 1995. *Proc. Natl. Acad. Sci. USA* 92:10384
64. Hudson JE, Abruna HD. 1996. *J. Am. Chem. Soc.* 118:6303
65. Green J-B, McDermott MT, Porter NM. 1996. *J. Phys. Chem.* 100:13342
66. Cleveland JP, Manne S, Bocek D, Hansma PK. 1993. *Rev. Sci. Instr.* 64:403
67. Hutter JL, Bechhoefer J. 1993. *Rev. Sci. Instr.* 64:1868
68. Senden TJ, Ducker WA. 1994. *Langmuir* 10:1003
69. Sader JE, Larson I, Mulvaney P, White LR. 1995. *Rev. Sci. Instr.* 66:3789
70. Warmack RJ, Zheng XY, Thundat T, Allison DP. 1994. *Rev. Sci. Instr.* 65:394
71. Neumeister JK, Ducker WA. 1994. *Rev. Sci. Instr.* 65:2527
72. Sader JE. 1995. *Rev. Sci. Instr.* 66:4583
73. Ogletree DF, Carprick RW, Salmeron M. 1996. *Rev. Sci. Instr.* 67:3298
74. Hazel J, Tsukruk VV. 1996. *Polym. Prepr.* 37:567
75. Marti O. 1993. *Phys. Scr. Vol. T* 49B:599
76. D'Costa NP, Hoh JH. 1995. *Rev. Sci. Instr.* 66:5096
77. Liu Y, Wu T, Fennel-Evans D. 1994. *Langmuir* 10:2241
78. Fujusawa S, Kishi E, Sugawara Y, Morita S. 1995. *Appl. Phys. Lett.* 66:526
79. Putman C, Igarashi M, Kaneko R. 1995. *Jpn. J. Appl. Phys.* 2:L264

80. Liu Y, Evans DF, Song Q, Grainger DW. 1996. *Langmuir* 12:1235
81. Schwarz UD, Koster P, Wiesendanger R. 1996. *Rev. Sci. Instr.* 67:2560
82. Griffith JE, Grigg DA, Vasile MJ, Russell PE, Fitzgerald EA. 1992. *J. Vac. Sci. Technol. A* 10:674
83. Sheiko SS, Moller M, Reuvekamp EMCM, Zandlbergen HW. 1993. *Phys. Rev. B* 48:5675
84. Atamny F, Baiker A. 1995. *Surf Sci.* 323:L314
85. Markiewicz P, Goh MC. 1995. *Rev. Sci. Instr.* 66:3186
86. Westra KL, Yeo YH, Thomson DJ, Mitchell AW. 1997. *J. Vac. Sci. Technol. A.* In press
87. Li Y, Lindsay SM. 1991. *Rev. Sci. Instr.* 62:2630
88. Odin C, Aime JP, El Kaakour Z, Bouhacina T. 1994. *Surf. Sci.* 317:321
89. Vesenka J, Manne S, Giberson R, Marsh T, Henderson E. 1993. *Biophys. J.* 65: 992
90. Vesenka J, Miller R, Henderson E. 1994. *Rev. Sci. Instr.* 65:2249
91. Han T, Williams JK, Bebbe TP Jr. 1995. *Anal. Chim. Acta* 307:365
92. Johnson KL, Kendall K, Roberts AD. 1971. *Proc. R. Soc. London Ser. A* 324: 301
93. Muller VK Yushchenko VS, Derjaguin BV. 1980. *J. Colloid Interface Sci.* 77: 91
94. Derjaguin BV, Muller VK, Toporov YP. 1975. *J. Colloid Interface Sci.* 53:314
95. Tabor D. 1977. *J. Colloid Interface Sci.* 58:2
96. Israelachvili JN, Perez E, Tandon RK. 1980. *J. Colloid Interface Sci.* 78:260
97. van Oss CJ, Chaudhury MK, Good RJ. 1988. *Chem. Rev.* 88:927
98. van Oss CJ, Good RJ, Chaudhury MK. 1988. *Langmuir* 4:884
99. Fowkes FM. 1962. *J. Phys. Chem.* 66:682
100. Lide DR. 1991. *CRC Handbook of Chemistry and Physics.* Boca Raton, FL: CRC Press
101. Lynch CT. 1975. *CRC Handbook of Materials Science.* Boca Raton, FL: CRC Press
102. Uman A. 1991. *Introduction to Ultrathin Organic Films.* New York: Academic
103. Terrill R, Postlethwaite T, Chen C, Poon C-D, Terzis A, et al. 1995. *J. Am. Chem. Soc.* 117:12537
104. Zhmud BV, Golub AA. 1994. *J. Colloid Interface Sci.* 167:186
105. Holmes-Farley SR, Reamey RH, McCarthy TJ, Deutch J, Whitesides GM. 1988. *Langmuir* 4:921
106. Creager SE, Clark J. 1994. *Langmuir* 10:3675
107. Chatelier R, Drummond C, Chan D, Vasic Z, Gengenbach T, et al. 1995. *Langmuir* 11:4122
108. Smart JL, McCammon JA. 1996. *J. Am. Chem. Soc.* 118:2283
109. Glinski GC, Platten JK, De Saedeleer C. 1993. *J. Colloid Interface Sci.* 162: 129
110. Lee TR, Carey RI, Biebuyck HA, Whitesides GM. 1994. *Langmuir* 10:741
111. Glinski J, Chavepeyer G, Platten JK, De Saedeleer C. 1993. *J. Colloid Interface Sci.* 158:382
112. Chavepeyer G, De Saedeleer C, Platten J. 1994. *J. Colloid Interface Sci.* 167:464
113. Yazdanian M, Yu H, Zografi G. 1990. *Langmuir* 6:1093
114. Larson D, Drummond CJ, Chan DYC, Grieser F. 1995. *J. Phys. Chem.* 99:2114
115. Meagher L, Pashley RM. 1995. *Langmuir* 11:4019
116. Reiner ES, Radke CJ. 1993. *Adv. Colloid Interface Sci.* 58:87
117. Manne S, Cleveland JP, Gaub HE, Stucky GD, Hansma PK. 1994. *Langmuir* 10:4409
118. Manne S, Gaub HE. 1995. *Science* 270:1480
119. Arai T, Aoki D, Okabe Y, Fujihira M. 1996. *Thin Solid Films.* 273:1
120. Overney RK, Takano H, Fujihira M, Paulus W, Ringsdorf H. 1994. *Phys. Rev. Lett.* 72:3546
121. Meyer E, Luthi R, Howald L, Barnmerlin K, Guggisberg M, et al. 1996. *J. Vac. Sci. Technol. B* 14:1285
122. Schumacher A, Kruse N, Prins R, Meyer E, Lijthi R, et al. 1996. *J. Vac. Sci. Technol. B* 14:1264
123. Scandella L, Meyer E, Howald L, Luthi R, Guggisberg M, et al. 1996. *J. Vac. Sci. Technol. B* 14:1255
124. Binggeli M, Mate CM. 1994. *Appl. Phys. Lett.* 65:415
125. Yoshizawa H, Israelachvili J. 1994. *Thin Solid Films* 246:1
126. Xiao XH, Charych DH, Salmeron M. 1996. *Langmuir* 12:235
127. Schwarz UD, Allers W, Gensterblum G, Wiesendanger R. 1995. *Phys. Rev. B* 52:14976
128. Carpick RW, Agrait N, Ogletree DF, Salmeron M. 1996. *J. Vac. Sci. Technol. B* 14:1289
129. Carpick RW, Agrait N, Ogletree DF, Salmeron M. 1996. *Langmuir* 12:3334
130. Marti A, Hahner G, Spencer ND. 1995. *Langmuir* 11:4632

131. Overney RM, Meyer E, Frommer J, Guntherodt H-J, Fujihira M, et al. 1994. *Langmuir* 10:1281
132. Berger CEH, van der Werf KO, Kooyman RPH, de Grooth BG, Greve J. 1995. *Langmuir* 11:4188
133. Koleske DD, Barger WR, Lee GU, Colton RJ. 1997. *Langmuir.* In press
134. Wollman EW, Kang D, Frisbie CD, Lorkovic IM, Wrighton MS. 1994. *J. Am. Chem. Soc.* 116:4395
135. Akari S, Horn D, Keller H, Schrepp W. 1995. *Adv. Mater.* 7:549
136. Akari S, Schrepp W, Horn D. 1996. *Langmuir* 12:857
137. Radmacher M, Tillmann RW, Fritz M, Gaub HE. 1992. *Science* 257:1900
138. Knapp BF, Wiegrabe W, Heim M, Eschrich R, Guckenberger R. 1995. *Biophys. J.* 69:708
139. Zhong Q, Inniss D, Kjoller K, Elings VB. 1993. *Surf. Sci.* 290:1
140. Hansma PK, Cleveland JP, Radmacher M, Walters DA, Hillner PE, et al. 1994. *Appl. Phys. Lett.* 64:1738
141. Howard AJ, Rye RR, Houston JE. 1996. *J. Appl. Phys.* 79:1885
142. Umemura K, Arakawa H, Ikai A. 1993. *Jpn. J. Appl. Phys.* 2:L1711
143. Turner DC, Chunyen C, Brandow SL, Murphy DB, Gaber BP. 1995. *Ultramicroscopy* 58:425
144. Leuba SH, Yang G, Robert C, Samori B, Van Holde K, et al. 1994. *Proc. Natl. Acad. Sci. USA* 91:11621
145. Radmacher M, Fritz M, Hansma PK. 1995. *Biophys. J.* 69:264
146. Hansma HG, Laney DE, Bezanilla M, Sinsheimer RL, Hansma PK. 1995. *Biophys. J.* 68:1672
147. Elings V, Gurley J. 1995. *U.S. Patent Nos. 5412980 and 5519212*